Developmental Cell
Article

HAND2 Targets Define a Network of Transcriptional Regulators that Compartmentalize the Early Limb Bud Mesenchyme

Marco Osterwalder,[1] Dario Speziale,[1] Malak Shoukry,[2] Rajiv Mohan,[3] Robert Ivanek,[1] Manuel Kohler,[4] Christian Beisel,[4] Xiaohui Wen,[5] Suzie J. Scales,[5] Vincent M. Christoffels,[3] Axel Visel,[2,6,7] Javier Lopez-Rios,[1,*] and Rolf Zeller[1,*]
[1]Developmental Genetics, Department of Biomedicine, University of Basel, 4058 Basel, Switzerland
[2]Genomics Division, MS 84-171, Lawrence Berkeley National Laboratory, Berkeley, CA 94720, USA
[3]Department of Anatomy, Embryology, and Physiology, Heart Failure Research Center, Academic Medical Center, University of Amsterdam, 1100 DD Amsterdam, the Netherlands
[4]Department for Biosystems Science and Engineering, Federal Institute of Technology Zurich, 4058 Basel, Switzerland
[5]Department of Molecular Biology, Genentech, Inc., 1 DNA Way, South San Francisco, CA 94080, USA
[6]U.S. Department of Energy Joint Genome Institute, Walnut Creek, CA 94598, USA
[7]School of Natural Sciences, University of California, Merced, Merced, CA 95343, USA
*Correspondence: javier.lopez-rios@unibas.ch (J.L.-R.), rolf.zeller@unibas.ch (R.Z.)
http://dx.doi.org/10.1016/j.devcel.2014.09.018

SUMMARY

The genetic networks that govern vertebrate development are well studied, but how the interactions of *trans*-acting factors with *cis*-regulatory modules (CRMs) are integrated into spatiotemporal regulation of gene expression is not clear. The transcriptional regulator HAND2 is required during limb, heart, and branchial arch development. Here, we identify the genomic regions enriched in HAND2 chromatin complexes from mouse embryos and limb buds. Then we analyze the HAND2 target CRMs in the genomic landscapes encoding transcriptional regulators required in early limb buds. HAND2 controls the expression of genes functioning in the proximal limb bud and orchestrates the establishment of anterior and posterior polarity of the nascent limb bud mesenchyme by impacting *Gli3* and *Tbx3* expression. TBX3 is required downstream of HAND2 to refine the posterior *Gli3* expression boundary. Our analysis uncovers the transcriptional circuits that function in establishing distinct mesenchymal compartments downstream of HAND2 and upstream of SHH signaling.

INTRODUCTION

The limb bud is an excellent model to study the gene networks that govern growth and patterning during vertebrate organogenesis (Zeller et al., 2009). These gene regulatory networks impact the expression of target genes via large *cis*-regulatory landscapes that integrate different inputs in a spatiotemporally controlled manner (Spitz and Furlong, 2012). For example, the expression of *Shh* in the posterior limb bud mesenchyme is controlled by a far upstream *cis*-regulatory module (CRM), termed ZRS (Lettice et al., 2003). Genetic ablation of the ZRS phenocopies the *Shh* loss of function in mouse limb buds, manifesting itself in loss of digits (Sagai et al., 2005). In contrast, point mutations in the highly conserved core underlie preaxial polydactyly in several species, including humans (Anderson et al., 2012). Localized *Shh* expression depends on the interaction of different transcriptional regulators with the ZRS. In particular, the interaction with HOX, PBX, ETS, and HAND2 transcriptional complexes has been implicated in activation of *Shh* in the limb bud, whereas TWIST1, ETV, and GATA factors prevent anterior ectopic expression (Capellini et al., 2006; Galli et al., 2010; Kmita et al., 2005; Kozhemyakina et al., 2014; Lettice et al., 2012, 2014; Mao et al., 2009; Zhang et al., 2009, 2010). How the ZRS integrates these various inputs over time is unknown, but the resulting posterior restriction of SHH signaling is essential for proliferative expansion and anterior-posterior (AP) patterning of the distal limb bud mesenchyme that will form the skeletal elements of the zeugopod and autopod (Ahn and Joyner, 2004; Chiang et al., 2001; Harfe et al., 2004; Zhu et al., 2008).

The mesenchymal progenitors giving rise to the most proximal skeletal structures (i.e., scapula and humerus in the forelimb) are likely specified prior to activation of SHH signaling (Ahn and Joyner, 2004; Dudley et al., 2002; Mariani et al., 2008; Mercader et al., 2000; Zeller et al., 2009). It has been shown that proximal mesenchymal progenitors express several transcriptional regulators belonging to the *Pbx*, *Meis*, and *Irx* gene families, which participate in specification and/or morphogenesis of proximal skeletal elements (Capdevila et al., 1999; Capellini et al., 2010; Li et al., 2014; Mercader et al., 2000; Selleri et al., 2001). Genetic evidence indicates that *Raldh2*, which is involved in retinoic acid synthesis, regulates the expression of several of these early genes, including the bHLH transcriptional regulator *Hand2* (Niederreither et al., 2002; Vitobello et al., 2011; Zhao et al., 2009).

Hand2 is genetically required for limb bud, branchial arch, and heart development and the lethality of *Hand2*-deficient mouse embryos around embryonic day E9.5 is caused by the severe heart malformations (Srivastava et al., 1997; Vincentz et al., 2011). During early limb bud development, *Hand2* is required for AP polarization of the nascent limb bud mesenchyme and activation of *Shh* expression as part of its genetic interactions with *Gli3* (Charité et al., 2000; Galli et al., 2010). In particular,

the *Hand2* and *Gli3* genetic antagonism is required to establish AP asymmetry and pentadactyly, as limb buds deficient for both these transcriptional regulators lack discernible AP polarity, *Shh* expression, and are extremely polydactylous (Galli et al., 2010; te Welscher et al., 2002). As inactivation of *Hand2* after the onset of *Shh* expression does not severely alter limb bud development, *Hand2* functions are required mostly upstream of activating SHH signaling (Galli et al., 2010). However, the molecular nature of the underlying transcriptional and *cis*-regulatory networks remained largely unknown, as *Shh* is the only known direct transcriptional target of HAND2 in limb buds.

We have inserted a 3xFLAG epitope tag into the endogenous HAND2 protein to first determine the range of genomic regions enriched in endogenous HAND2 chromatin complexes. In a second step, we focused our in-depth analysis predominantly on HAND2 target genes that encode transcription factors expressed and/or required during early limb development. This analysis established that during the onset of limb bud outgrowth, HAND2 controls the expression of transcriptional regulators in the proximal mesenchyme that are involved in the formation of the most proximal forelimb skeletal elements. In addition, our study reveals the gene regulatory logic by which HAND2, in cooperation with GLI3 and TBX3, establishes AP axis polarity in the early limb bud mesenchyme. In summary, our analysis uncovers the HAND2-dependent molecular circuits that function in establishing proximal, anterior, and posterior compartments and activating *Shh* expression during the onset of limb bud development.

RESULTS

A *Hand2*^{3xFLAG} Allele Generated by dRMCE Identifies the Genomic Regions Enriched in Endogenous HAND2 Chromatin Complexes

A 3xFLAG epitope tag was inserted into the endogenous HAND2 protein using dual recombinase-mediated cassette exchange (dRMCE; Osterwalder et al., 2010) to replace the conditional allele with a *Hand2*^{3xFLAG} cassette in mouse embryonic stem cells (ES) (Figure 1A; Supplemental Experimental Procedures available online). Insertion of the 3xFLAG epitope tag into the N terminus does not alter HAND2 functions, as homozygous *Hand2*^{3xFLAG} (*Hand2*$^{3xF/3xF}$) mice develop normally and do not show any embryonic lethality (Galli et al., 2010; Srivastava et al., 1997; data not shown). The 3xFLAG epitope tag allows sensitive detection of the endogenous HAND2 protein isoforms in embryonic tissues (limb buds, heart, and branchial arches; Figures 1B and 1C). During the onset of forelimb bud outgrowth, HAND2-positive nuclei are detected in the posterior and proximal-anterior limb bud mesenchyme (green fluorescence; Figures 1D, S1A, and S1D). As HAND2 is required to activate *Shh* expression (Galli et al., 2010), we compared the distribution of HAND2-positive and *Shh*-expressing cells using the *Shh*-GFP allele (red fluorescence; Harfe et al., 2004). The *Shh*-expressing cells define a subdomain within the posterior HAND2-positive limb bud mesenchyme (Figures 1D and S1D). We also colocalized HAND2 with the GLI3 repressor isoform (GLI3R) to determine their spatial distribution during activation of *Shh* expression. GLI3R proteins were detected by immunofluorescence using monoclonal GLI3 N-terminal antibodies (Wen et al., 2010) as they recognize the nuclear GLI3R isoform rather than the cytoplasmic full-length GLI3 and/or nuclear GLI3A activator isoforms in limb bud sections (Figures S1B and S1C). This analysis reveals the complementary distribution of the nuclear HAND2 (green) and GLI3R proteins (purple) in mouse forelimb bud mesenchymal cells (Figures 1D, S1B, and S1D).

The only known direct target of HAND2 in limb buds is *Shh*, whose transcriptional activation is controlled by interaction of HAND2 with the ZRS *cis*-regulatory region located ~800 kb upstream of the *Shh* locus (Galli et al., 2010; Lettice et al., 2003). *Hand2*$^{3xF/3xF}$ limb buds were used for chromatin immunoprecipitation (ChIP) using anti-FLAG antibodies in combination with quantitative real-time PCR (ChIP-qPCR). While our previous analysis did not unambiguously identify the HAND2-binding region(s) within the ZRS (Galli et al., 2010), ChIP of the endogenous HAND2^{3xF} epitope-tagged protein resulted in identification of a specific region within the ZRS (Figure 1E). Amplicon-tiling of the ZRS core (~1.1 kb; Sagai et al., 2005) showed that a region encoding an *Ebox* is most enriched in HAND2 chromatin complexes (ZRS2-4 in Figure 1E; Dai and Cserjesi, 2002). This interaction is specific, as another *Ebox* sequence is not enriched (ZRS5; Figure 1E). The enrichment of the ZRS2-4 region in HAND2 chromatin complexes is highest in early limb buds (E10.5; Figure 1E) in agreement with the early but transient genetic requirement of *Hand2* for *Shh* activation ($\leq$E10.5; Galli et al., 2010).

To define the range of potential HAND2 targets during its early genetic requirement in mouse limb buds, we used chromatin immunoprecipitation sequencing (ChIP-seq). To this aim, the HAND2 binding profile in *Hand2*-expressing embryonic tissues at E10.5 (eT, limb buds and flank tissue, hearts, and branchial arches; Figure 1B) and dissected limb buds (Lb) was determined by HAND2^{3xF} ChIP-seq analysis (Figures 2A–2D and S2A). The primary data sets were analyzed using model-based analysis for ChIP-seq (MACS)-based peak calling, and regions enriched in wild-type eT controls were excluded as nonspecific (Tables S1 and S2 list all statistically validated regions enriched $\geq$2-fold). For both validated ChIP-seq data sets, the top 1,000 peaks were selected for the initial meta-analysis based on their fold enrichment over the input control and number of reads (Figures 2A–2D and S2A; Tables S3 and S4). The majority of the top 1,000 HAND2-binding peaks in both data sets map to conserved sequences located $\geq$10 kb away from the closest transcriptional start site (TSS; Figures 2A and 2B). De novo motif discovery showed that also the endogenous HAND2 chromatin complexes interact preferentially with the *Ebox* sequence defined in vitro (Figure 2C; Dai and Cserjesi, 2002).

Intersection of the top 1,000 eT and Lb data sets shows that 259 of them are shared (Figure S2A; Table S5). GREAT analysis showed that the shared HAND2-binding regions are most often associated with genes known to function in limb bud and/or skeletal development (Figures 2D and S2B). Hence, this set of shared regions and associated genes likely corresponds to HAND2 target genes in limb buds. However, it is important to consider that the sequence coverage was overall significantly lower for the Lb than for the eT ChIP-seq data set. This is a likely consequence of the much lower amounts of tissue and HAND2 chromatin complexes recovered from the ~1,000 fine-dissected limb buds used for ChIP-seq analysis (Supplemental Experimental Procedures). Furthermore, the ZRS, which is an

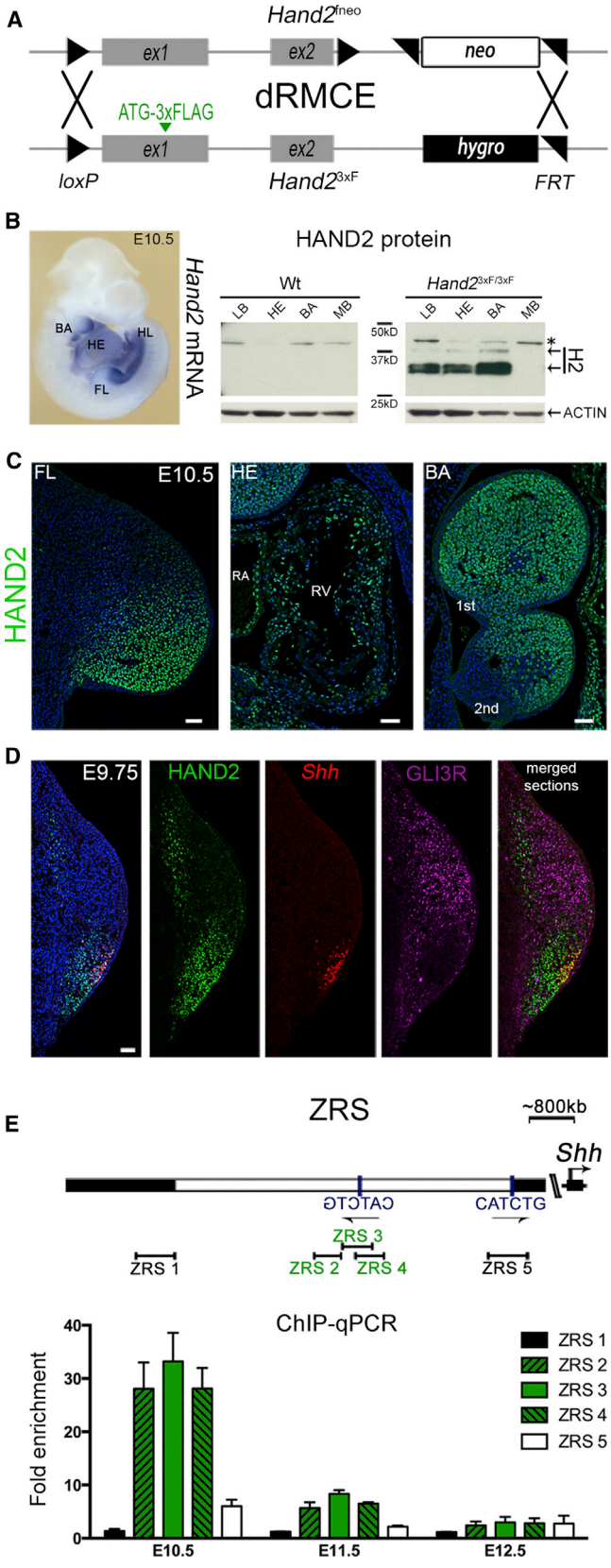

Figure 1. Insertion of a 3xFLAG Epitope Tag into the Endogenous HAND2 Protein Provides a Sensitive Tool to Detect HAND2 Protein Complexes

(A) The *Hand2*^{3xF} allele was generated by dRMCE in mouse ES cells.

(B) Left: *Hand2*-expressing tissues in mouse embryos at embryonic day E10.5. Right: immunoblot detection of the tagged HAND2^{3xF} protein isoforms (H2) in limb buds (LB), heart (HE), and branchial arches (BA). Midbrain (MB) and wild-type extracts are used as negative controls. An asterisk indicates a nonspecific band. FL, forelimb bud; HL, hindlimb bud.

(C) Detection of HAND2^{3xF} proteins in expressing embryonic tissues by immunofluorescence (green) at E10.5. RV, right ventricle; RA, right atrium. 1st, mandibular arch; 2nd, hyoid arch.

(D) Colocalization of HAND2^{3xF} proteins (green) and *Shh* transcripts (red) in limb buds (E9.75, 28–29 somites). The distribution of nuclear GLI3R proteins (magenta) is shown on an adjacent section. The right-most panel shows an artificial overlap of the two consecutive sections. Limb buds are always oriented with anterior to the top and posterior to the bottom. Nuclei are blue because of counterstaining with Hoechst. Scale bars, 50 μm.

(E) ChIP-qPCR analysis shows the interaction of HAND2^{3xF} chromatin complexes with a specific region in the ZRS in developing limb buds (E10.5, E11.5, and E12.5). The *Ebox* core sequence (CATCTG) defined by in vitro analysis is indicated. The most relevant qPCR amplicons used are indicated as ZRS 1–ZRS 5. Fold enrichment is shown as mean ± SD (n = 3).

See also Figure S1.

established HAND2 target region (Figure 1E), was moderately enriched only in the eT ChIP-seq data set (Table S4). This could reflect the fact that the HAND2-ZRS interaction occurs only in a small fraction of posterior mesenchymal cells in early limb buds, and ChIP-qPCR analysis relying on specific oligos is more sensitive (Figures 1D and 1E). The limited sensitivity of the Lb ChIP-seq data set, in particular, indicates that not all relevant HAND2 binding peaks have been detected and represented in the top 1,000 peaks used for the comparative analysis. This is likely a consequence of a significant fraction of HAND2 target genes being restricted very proximally in early limb buds and extending into the flank mesenchyme (see below). However, the flank mesenchyme was only included in the eT, but not in the Lb ChIP-seq sample. Therefore, all potential HAND2 target regions selected for further analysis were first verified in early limb buds (E10.5), using the more sensitive HAND2 ChIP-qPCR analysis (n = 3; Experimental Procedures).

As we mainly wanted to get insight into the transcriptional circuitry controlled by HAND2 during prepatterning of early limb buds (te Welscher et al., 2002), the current study focused on the genomic regions associated with transcription factors functioning and/or expressed upstream of activating *Shh* expression. To assess the expression of the associated genes in mutant mouse limb buds, *Hand2* was conditionally deleted during limb bud initiation using the *Hoxb6*-Cre transgene (Lowe et al., 2000). This inactivates *Hand2* in the posterior two-thirds of the forelimb bud mesenchyme (Figures S2C and S2D), resulting in almost complete penetrance of the *Hand2* loss-of-function limb bud phenotype (n = 9/10). Our initial analysis of the curated list of genes expressed and/or functioning in early limb buds showed that most often their expression is altered in the posterior-proximal mesenchyme of *Hand2*$^{\Delta/\Delta c}$ forelimb buds (≤E10.25; n = 17/29 genes analyzed; Table 1). Their expression is either significantly reduced or lost from the posterior mesenchyme (n = 10/17; including *Ets1, Ets2*, *Gsc*, *Tbx2*, and *Tbx3*; Table 1; Figure S2E) or expands posteriorly (n = 7/17; including

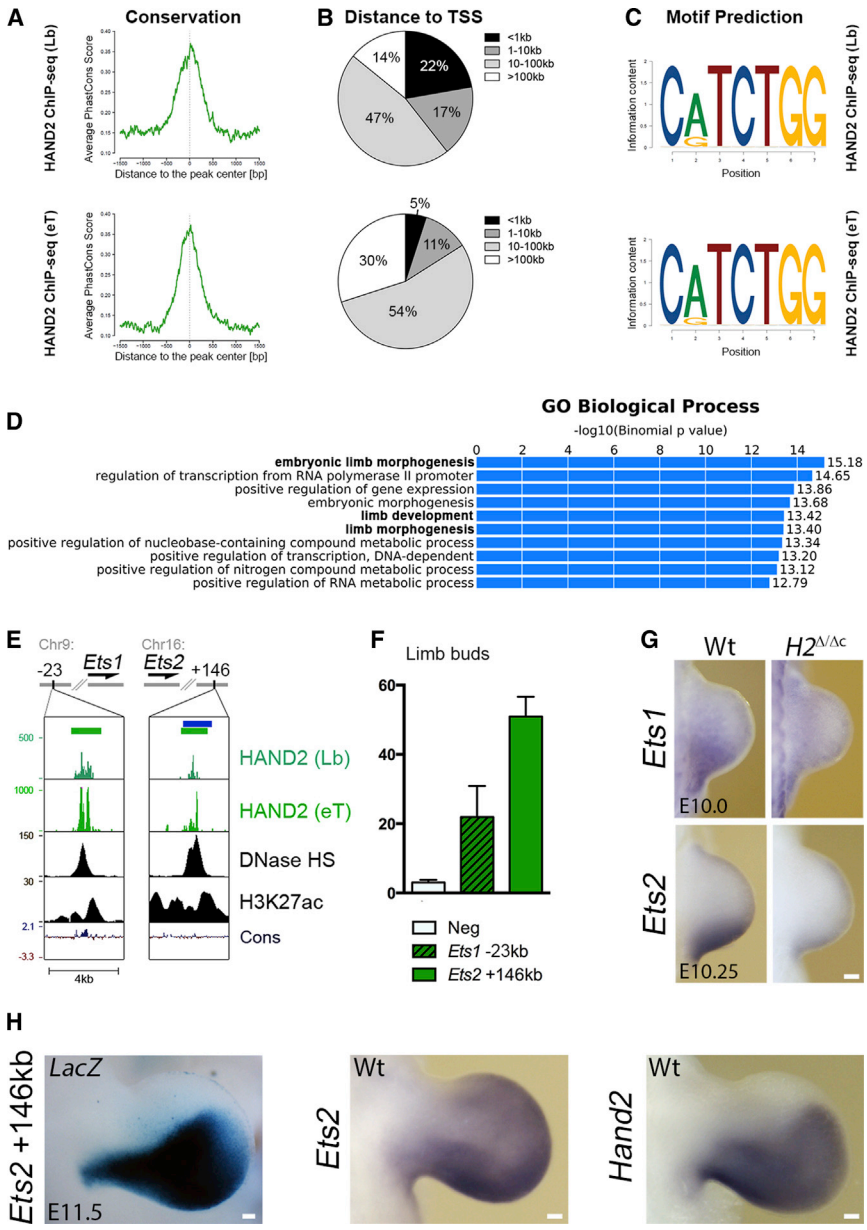

Figure 2. ChIP-Seq Analysis Identifies a Set of HAND2 Target Regions in Mouse Limb Buds

(A and B) The top 1,000 HAND2^{3xF} target regions enriched in E10.5 limb buds (Lb) and *Hand2*-expressing embryonic tissues (eT) are mostly evolutionarily conserved (A) and map generally ≥10kb away from the closest transcriptional start site (TSS; B).

(C) De novo motif discovery analysis of the top 1,000 HAND2^{3xF} bound regions reveals enrichment in *Ebox* consensus sequences.

(D) Gene ontology (GO) analysis reveals the most prominent biological processes associated with HAND2^{3xF} binding regions that are represented in both top 1,000 Lb and eT data sets.

(E) UCSC Genome Browser window shows the *Ets1* and *Ets2* regions enriched in HAND2 chromatin complexes from limb buds (Lb) and expressing tissues (eT). Distances to the *Ets1 and Ets2* TSS are indicated in kilobases. The profiles of DNaseI HS and H3K27ac marks in limb buds (E11.5) are shown in black (Cotney et al., 2012). The placental mammal conservation (Cons) plot (PhyloP) is shown below. Green bars represent the peaks identified by MACS analysis. The blue bar indicates the hs1516 enhancer element assayed by *LacZ* transgenesis (Vista Enhancer Browser). The ChIP-seq panels in all figures are organized the same.

(F) ChIP-qPCR statistically verifies the HAND2^{3xF} binding regions in the *Ets1* and *Ets2* genomic landscapes in limb buds (n = 3; E10.5). Mean ± SD is shown.

(G) *Ets1* and *Ets2* transcript distribution in wild-type and *Hand2*$^{\Delta/\Delta c}$ forelimb buds (≤E10.25).

(H) The activity of the *Ets2* +146kb human ortholog (hs1516-*LacZ* reporter, Vista Enhancer Browser) is compared with the endogenous *Ets2* and *Hand2* expression in forelimb buds (E11.5). Scale bars, 100 μm.

See also Figure S2 and Tables S1, S2, S3, S4, and S5.

Gli3, *Tbx18*, *Irx3*, and *Irx5*; Table 1; Figure S2F). This initial analysis pointed to the existence of a network of transcriptional regulators that are direct targets of HAND2 during the onset of limb bud development (Table 1; data not shown).

For example, two candidate CRMs located 23 kb upstream of the *Ets1* and 146 kb downstream of the *Ets2* TSS are significantly enriched in HAND2^{3xF} chromatin complexes as confirmed by ChIP-qPCR in early limb buds (Figures 2E and 2F). Indeed, the expression of both *Ets1* and *Ets2* is reduced in *Hand2*-deficient limb buds (Figure 2G). The *Ets2* +146kb CRM likely encodes an enhancer as the orthologous human region is active in the posterior limb bud mesenchyme of transgenic mouse embryos (Figure 2H, left panel; Vista enhancer hs1516; Visel et al., 2007). The domain of the *LacZ* reporter not only recapitulates major aspects of *Ets2* expression (Figure 2H, middle panel) but also overlaps the endogenous *Hand2* domain (Figure 2H, right panel). These results establish the *Ets1* and *Ets2* genes as bona fide HAND2 target genes in early limb buds. As the *ETS* binding sites in the ZRS are essential for *Shh* expression in the posterior limb bud (Lettice et al., 2012, 2014), HAND2-mediated upregulation of the *Ets* transcription factors likely helps to reinforce *Shh* expression.

HAND2 Target Genes Are Required in the Proximal Limb Bud for Morphogenesis of the Scapula and Humerus

As part of the initial analysis, HAND2 peaks were detected in the genomic landscapes of several transcription factors expressed in the proximal limb bud mesenchyme (Figure 3; Table 1) and that function in morphogenesis of proximal limb skeletal elements (scapula and humerus; Belo et al., 1998; Farin, 2009; Li et al., 2014). In particular, two prominent HAND2 peaks, whose enrichment in early limb buds was confirmed by ChIP-qPCR, map to the *Goosecoid* (*Gsc*) genomic landscape (at positions +33

Table 1. Summary of the RNA In Situ Hybridization Analysis of a Select Set of HAND2 Target Genes in *Hand2*-Deficient Limb Buds

	Genes
Upregulated	*Alx4*,[a] *Gas1*, *Gli3*, *Irx3*, *Irx5*, *Msx2*,[a] *Tbx18*
Downregulated	*Ets1*, *Ets2*, *Furin*, *Gsc*, *Shh*,[b] *Slit3*, *Tbx2*, *Tbx3*, *Unc5c*, *Zfp503*
Not changed	*Bmp4*,[a] *Bmp7*, *Cyp26b1*, *Fgfr1*, *Gli2*, *Lmx1b*, *Meis2*, *Msx1*, *Mycn*, *Snai1*, *Tbx4*, *Tbx5*

Validated ChIP-seq peaks associated with genes encoding transcriptional regulators and/or essential roles during the onset of mouse limb bud development were selected. This table summarizes the alterations in their expression in *Hand2*-deficient mouse forelimb buds (≤E10.5). Genomic landscapes associated with genes functioning during progression of limb bud development and genes expressed either in the limb bud ectoderm or during advanced stages (e.g., chondrogenesis) were not considered for this study.
[a]Genes analyzed by Galli et al. (2010).
[b]Only enriched in the eT ChIP-seq data set.

and −133 kb; Figure 3A). *Gsc* is expressed in the proximal and flank mesenchyme during early limb bud development and is required for scapular head development in the mouse (Belo et al., 1998). In agreement with *Gsc* being a direct transcriptional target of HAND2, its expression is lost from the posterior mesenchyme of *Hand2*$^{\Delta/\Delta c}$ forelimb buds (Figure 3A). Genetic analysis underscores the functional importance of *Gsc* regulation by HAND2, as *Hand2*$^{\Delta/\Delta c}$ and *Gsc*-deficient limbs display strikingly similar scapular defects affecting the glenoid cavity and coracoid process (n = 4/8; Figures 3B and S3A; compare to Belo et al., 1998). In limb buds, HAND2 chromatin complexes also interact with a specific region in the *Tbx18* genomic landscape (at position −338 kb; middle panel, Figure 3C). Indeed, *Tbx18* expression expands posteriorly in *Hand2*$^{\Delta/\Delta c}$ forelimb buds (Figure 3C), and previous genetic analysis established that *Tbx18* also functions during scapula and humerus development (Farin, 2009).

Recently, it has been shown that the *Irx3* and *Irx5* transcriptional regulators, which are part of the same gene cluster (Figure 3D), are required to specify the progenitors of proximal and anterior limb skeletal elements during limb bud initiation (Li et al., 2014). Interestingly, HAND2 chromatin complexes bind to a region located 85 kb downstream of the *Irx3* TSS and adjacent to a GLI3R binding region (red bar in Figure 3D; Vokes et al., 2008). *Irx3* and *Irx5* are likely part of the same *cis*-regulatory landscape as they are coexpressed in the anterior-proximal limb bud mesenchyme and their expression expands posteriorly in *Hand2*$^{\Delta/\Delta c}$ forelimb buds (Figure 3E). As this region encompasses binding regions for both HAND2 and GLI3R chromatin complexes, its enhancer potential (blue bar in Figure 3D) was assessed in transgenic mouse embryos (Figure 3F). Indeed, this region functions as a CRM in limb buds, but the mesenchymal *LacZ* reporter activity is rather uniform in contrast to the proximal-anterior restriction of the endogenous *Irx3* and *Irx5* expression domains (n = 10/10; Figure 3F). Furthermore, as the GLI3R binding regions in limb buds (Vokes et al., 2008) often map close to the ones for HAND2 (red bars in Figures 3A, 3C, and 3D; see also Figure S3B), the expression of these proximal genes was also analyzed in limb buds lacking both *Hand2* and *Gli3* (Figures S3C and S3D). While *Tbx18* expression is not significantly altered, the expression of *Gsc* and *Irx3* is much more reduced in double than in wild-type or in single mutant limb buds (Figures S3C and S3D; data not shown). These alterations in gene expression are paralleled by a more severely dysplastic scapula and humerus in *Hand2*$^{\Delta/\Delta c}$*Gli3*$^{\Delta/\Delta}$ limbs (Figure S3E). Together, these results indicate that HAND2 acts in concert with GLI3R to control a transcriptional network that functions in morphogenesis of proximal limb skeletal elements.

Direct Cross-Regulation between HAND2 and GLI3R Underlies Molecular Establishment of an Anterior and Posterior Limb Bud Compartment

Genetic analysis has shown that *Hand2* and *Gli3* are mutually antagonistic, and this has been proposed to prepattern the limb bud mesenchyme along its AP axis prior to activation of SHH signaling (Galli et al., 2010; te Welscher et al., 2002). *Hand2* is initially expressed uniformly throughout the limb field mesenchyme, but its expression becomes rapidly posteriorly restricted as *Gli3* is activated in the anterior margin (Charité et al., 2000; te Welscher et al., 2002). At this early stage, the full-length cytoplasmic GLI3 protein is constitutively processed to GLI3R, which translocates to the nucleus in the absence of SHH signaling (Figure S4; Wang et al., 2000). To gain insight into the underlying molecular and cellular interactions, we colocalized the endogenous HAND2^{3xF} and GLI3R proteins during forelimb bud formation (E9.25; Figure 4A). HAND2 protein levels are highest in posterior and proximal-anterior nuclei (green fluorescence; Figure 4A), whereas GLI3R is most abundant in anterior nuclei (red fluorescence, Figure 4A). In spite of their opposing distribution, most mesenchymal cells coexpress nuclear HAND2 and GLI3R proteins during forelimb bud formation (yellow overlap; n = 4/4 at E9.25; Figures 4A and S5A). Subsequently, HAND2 becomes undetectable in anterior cells, which retain GLI3R. Conversely, GLI3R is lost from posterior cell nuclei, which retain HAND2 (n = 3/3 at E9.5-9.75; Figures 4B and S5B). Cells at the interface of the two domains continue to coexpress both proteins (Figures 4B and S5B). These spatial dynamics reveal how the populations of GLI3R-positive anterior and HAND2-positive posterior cells segregate, likely concurrently with molecular establishment of AP axis polarity in forelimb buds. The SHH-independent nature of these interactions is revealed by the fact that the HAND2 and GLI3R domains are initially normal in *Shh*-deficient limb buds (E9.5–9.75; Figure S5C). During progression of forelimb bud outgrowth, the HAND2 and GLI3R domains are increasingly separated by cells expressing neither of these proteins (n = 3/3 at E10.25; Figure 4B), which likely reflects the inhibition of GLI3R formation by SHH signaling. As the two proteins are initially coexpressed, direct cross-regulation could underlie establishment of the mutually exclusive HAND2 and GLI3R domains. Indeed, GLI3R interacts with two CRMs in the *Hand2* genomic landscape that function in repressing *Hand2* from the anterior limb bud mesenchyme (Vokes et al., 2008). The CRM at position +13 kb is associated with one overlapping and a close-by region (at +11 kb) enriched in HAND2 chromatin complexes from limb buds (Figures S5D and S5E). This indicates that in addition to mediating repression by GLI3R, this CRM could also participate in autoregulation of *Hand2* expression.

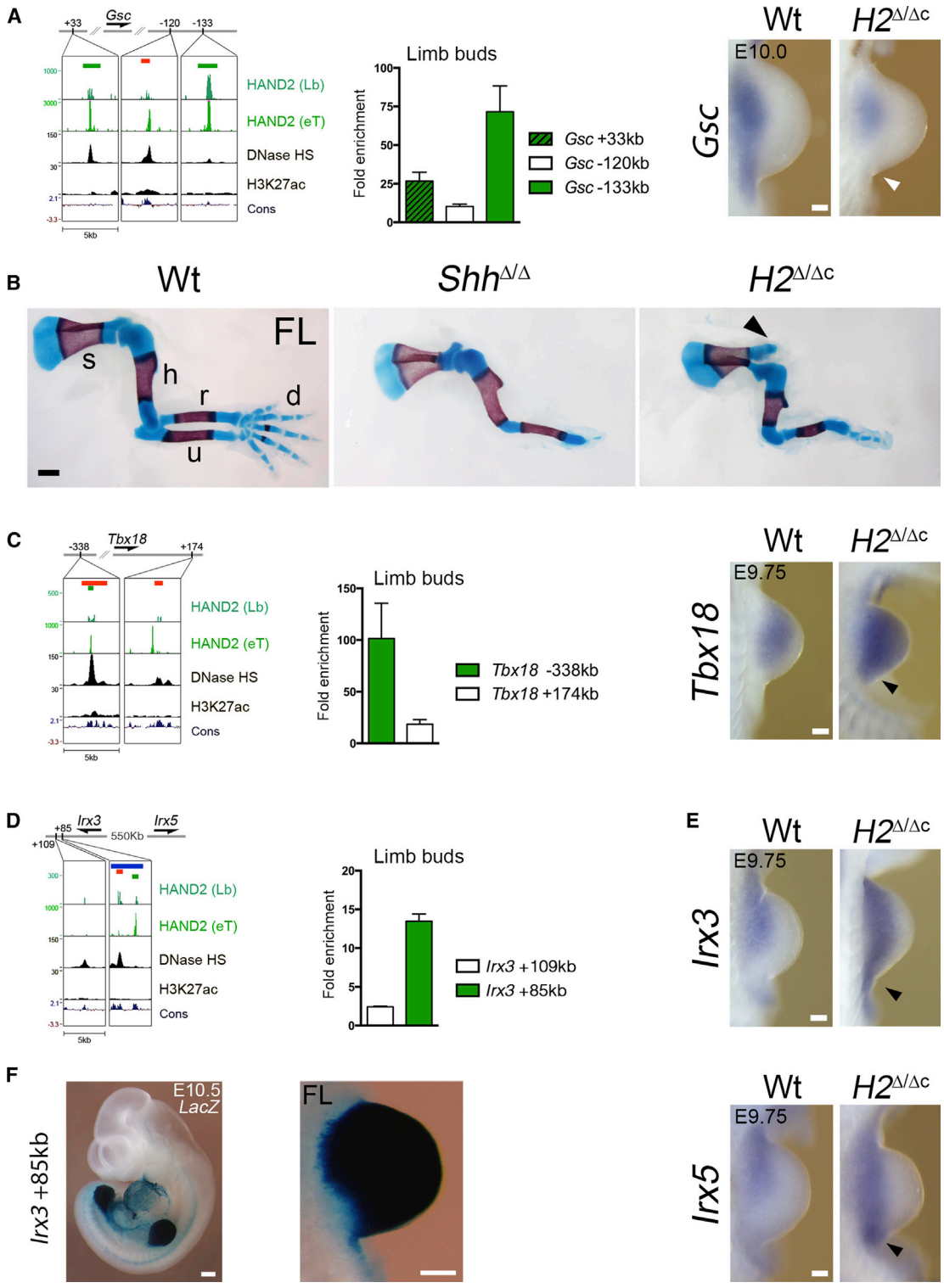

Figure 3. HAND2 Directly Regulates Genes Participating in Proximal Limb Bud Development

(A) Left: HAND2^{3xF} ChIP profiles in the genomic landscape encoding the *Gsc* transcriptional regulator (left panel). Green bars: HAND2 ChIP-seq peaks identified by MACS analysis. Red bar: genomic region interacting with GLI3R in limb buds (Vokes et al., 2008). Middle panel: HAND2 ChIP-qPCR analysis establishes the significant enrichment of the *Gsc* +33 kb and *Gsc* −133 kb regions in limb buds (E10.5). Mean ± SD (n=3). Right: *Gsc* expression in wild-type and *Hand2*$^{\Delta/\Delta c}$ forelimb buds (E10.0, 30–31 somites). White arrowhead points to loss of *Gsc* expression from the posterior mesenchyme. Scale bar, 100 μm.

(legend continued on next page)

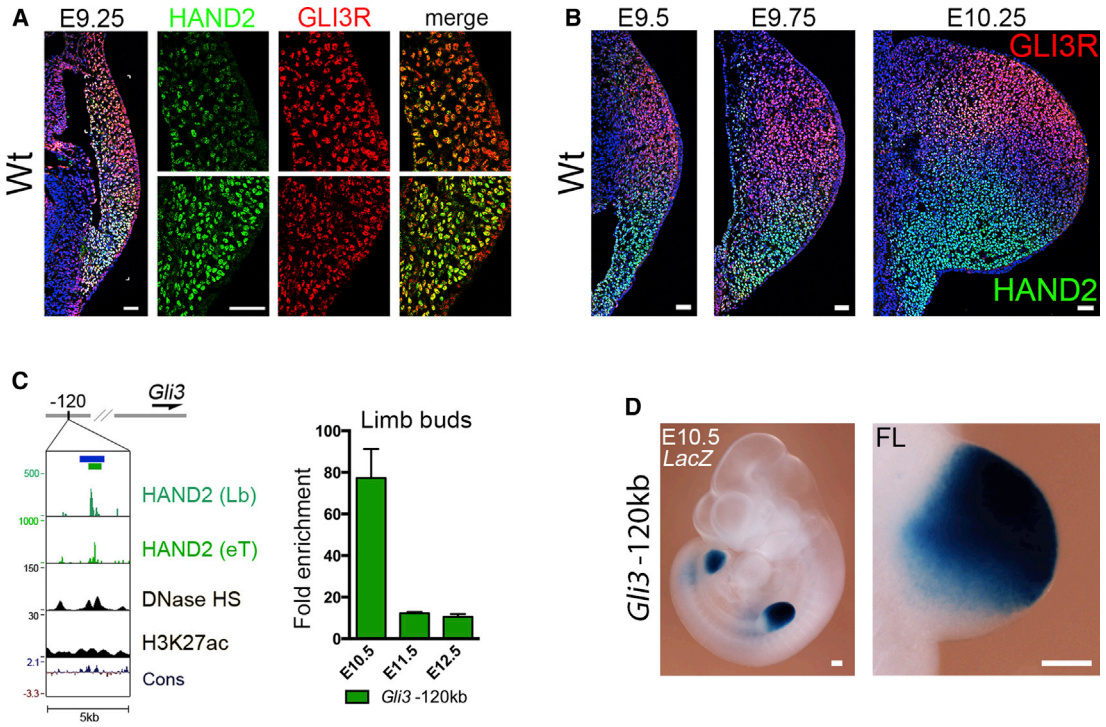

Figure 4. The Dynamics of the HAND2 and GLI3R Distributions Reveal the Establishment of a Posterior and Anterior Limb Bud Compartment

(A and B) Coimmunolocalization of HAND2^{3xF} (green) and GLI3R (red) in wild-type forelimb buds at E9.25 (22–23 somites), E9.5 (25–26 somites), E9.75 (28–29 somites), and E10.25 (32–33 somites). Scale bars, 50 μm.

(C) HAND2^{3xF} binding regions in the *Gli3* genomic landscape revealed by ChIP-seq analysis (green). Blue bar demarcates the *Gli3* −120 kb region chosen for *LacZ* reporter analysis. The right panel shows the temporal occupancy of the *Gli3* −120 kb region by HAND2 complexes as revealed by ChIP-qPCR analysis of limb buds from E10.5–E12.5. Mean ± SD is indicated (n = 3).

(D) Expression of the *LacZ* reporter under control of the *Gli3* −120 kb HAND2 binding region in a transgenic embryo (E10.5) FL, forelimb bud. Scale bars, 200 μm.

See also Figures S4 and S5.

As *Gli3* expression expands posteriorly in *Hand2*-deficient mouse limb buds (Galli et al., 2010; te Welscher et al., 2002), we screened also the *Gli3* genomic landscape for HAND2-interacting regions (Figure 4C). Indeed, a region located 120 kb upstream of the *Gli3* transcription unit is prominently enriched in early limb buds (right panel, Figure 4C). Transgenic analysis showed that this CRM is indeed active both in fore- and hindlimb buds (Figure 4D). In particular, this CRM is able to drive *LacZ* expression in a spatial pattern reminiscent of the endogenous *Gli3* transcript distribution, with *LacZ* being excluded from the most posterior mesenchyme (n = 6/7; Figure 4D; data not shown).

Tbx3 Is a HAND2 Target Gene that Positions the Posterior *Gli3* Expression Boundary

HAND2 chromatin complexes are also enriched in two specific regions of the *Tbx3* genomic landscape that is required for expression in limb buds (Figures 5A and 5B; Horsthuis et al., 2009). While the eT and Lb HAND2 ChIP-seq data sets do not unequivocally identify the two regions for the reasons stated above, HAND2 ChIP-qPCR using early limb buds established that the region located 58 kb upstream of the *Tbx3* transcription unit is ~3-fold more enriched than the one located at −19 kb (left panel, Figure 5B). The enrichment of the *Tbx3* −58 kb region is most prominent in early limb buds

(B) Forelimb skeletons (FL) at E16.5 with cartilage in blue and bone in red. Arrowhead points to the malformed scapular head. s, scapula; h, humerus; r, radius; u, ulna; d, digits. Scale bar, 500 μm.

(C) Left: HAND2^{3xF} ChIP profiles in the genomic landscape encoding the *Tbx18* transcriptional regulator (left panel). Middle panel: HAND2 ChIP-qPCR analysis establishes the significant enrichment of the *Tbx18* −338 kb region in limb buds (E10.5). Mean ± SD (n=3). Right: *Tbx18* expression expands to the posterior in *Hand2*$^{\Delta/\Delta c}$ forelimb buds (black arrowhead, E9.75, 28–29 somites). Scale bar, 100 μm.

(D) Left: HAND2^{3xF} ChIP profiles in the genomic landscape encoding the *Irx3* and *Irx5* transcriptional regulators. Blue bar: genomic region tested for enhancer activity in mouse transgenic embryos. Right: HAND2 ChIP-qPCR analysis establishes the significant enrichment of the *Irx3* +85 kb region in limb buds (E10.5). Mean ± SD (n=3).

(E) The expression of *Irx3* and *Irx5* expands posteriorly in *Hand2*$^{\Delta/\Delta c}$ forelimb buds (black arrowhead, E9.75, 28–29 somites). Scale bar, 100 μm.

(F) Expression of the *LacZ* reporter under control of the *Irx3* +85 kb CRM in a representative transgenic mouse embryo (E10.5) FL, forelimb bud. Scale bars, 200 μm.

See also Figure S3.

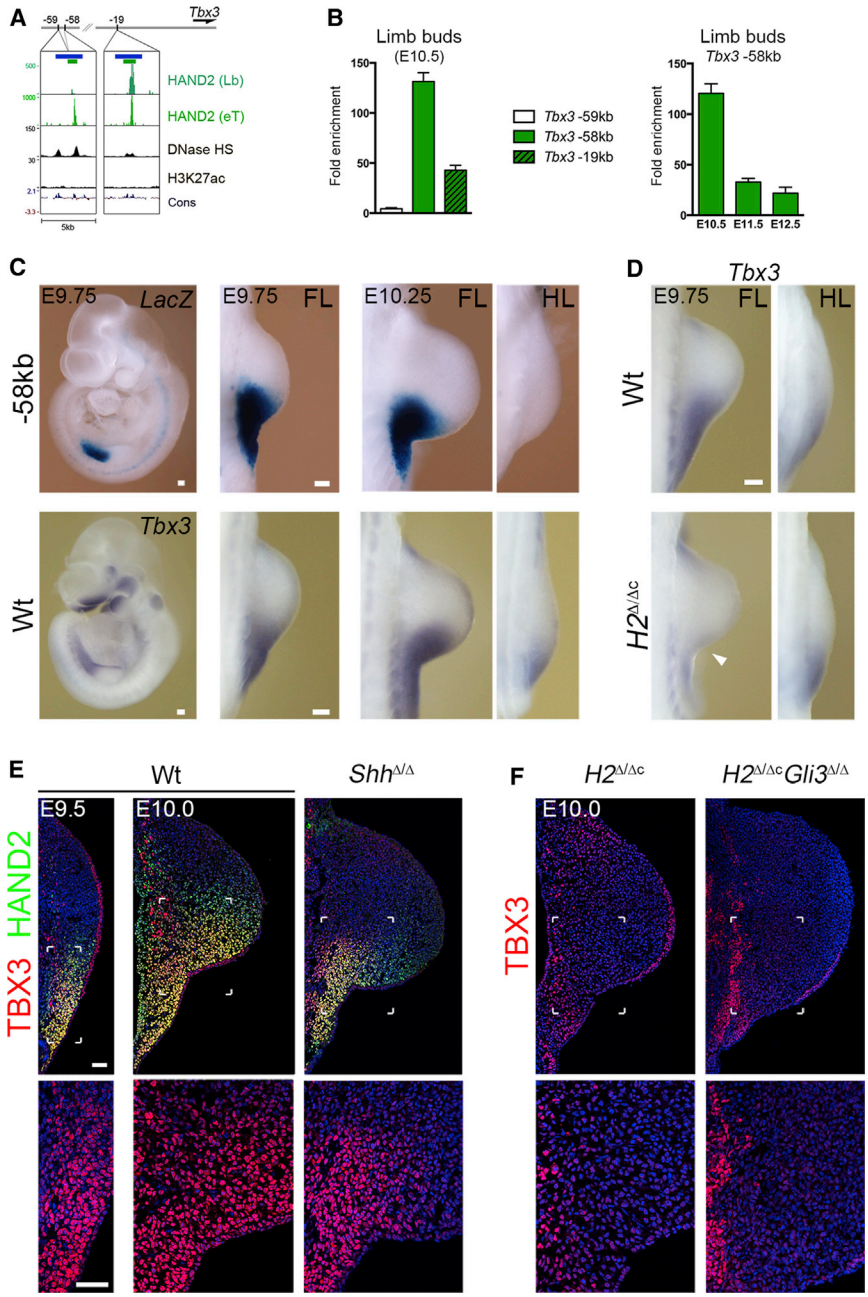

Figure 5. HAND2 Controls *Tbx3* Expression by Interacting with a CRM that Is Active Early in the Posterior Forelimb Bud Mesenchyme

(A) HAND2^{3xF} binding regions in the *Tbx3* locus as defined by ChIP-seq analysis.

(B) Left: ChIP-qPCR reveals the significance of the interactions of HAND2^{3xF} chromatin complexes with the *Tbx3* −58 kb and *Tbx3* −19 kb regions in limb buds (E10.5). Mean ± SD (n = 3). Right: temporal dynamics of the occupancy of the *Tbx3* −58 kb region by HAND2^{3xF} complexes in limb buds.

(C) Upper: expression of *LacZ* under control of the *Tbx3* −58 kb HAND2 binding region in transgenic embryos at E9.75 and E10.25. Lower: endogenous *Tbx3* transcript distribution in wild-type embryos. FL, forelimb bud; HL, hindlimb bud. Scale bars, 100 μm.

(D) *Tbx3* expression in wild-type and *Hand2*$^{\Delta/\Delta c}$ fore- (FL) and hindlimb (HL) buds at E9.75. White arrowhead, loss of *Tbx3* in the posterior forelimb bud mesenchyme. Scale bar, 100 μm.

(E) Colocalization of the nuclear HAND2^{3xF} (green) and TBX3 (red) proteins in wild-type and *Shh*-deficient forelimb buds (E9.5, 25–26 somites; E10.0, 30–31 somites). Lower panels show enlargements of the posterior TBX3 protein domains.

(F) TBX3 protein distribution in *Hand2*$^{\Delta/\Delta c}$ and *Hand2*$^{\Delta/\Delta c}$ *Gli3*$^{\Delta/\Delta}$ forelimb buds (E10.0, 30–31 somites).

See also Figure S6.

(right panel, Figure 5B), pointing to an involvement of HAND2 in regulating the early *Tbx3* expression. This was corroborated by transgenic analysis, which established that the *Tbx3* −58 kb CRM drives *LacZ* expression in the posterior-proximal forelimb bud and flank mesenchyme in a pattern strikingly similar to the endogenous *Tbx3* expression (n = 8/10; Figures 5C and S6A). In contrast, the *Tbx3* −19 kb region is not active in mouse limb buds (n = 0/7; Figure S6A). The *Tbx3* −58 kb CRM regulates *Tbx3* expression during early limb bud development, as the *LacZ* expression domain fails to expand distally as limb bud development progresses (Figure S6A). As neither of the two HAND2 binding regions is active in hindlimb buds (Figures 5C and S6A; data not shown), the expression of *Tbx3* in hindlimb buds must be controlled by different *cis*-regulatory interactions.

Indeed, *Tbx3* expression is lost from the posterior mesenchyme of *Hand2*-deficient forelimb buds, while it remains comparable to wild-types in mutant hindlimb buds (Figure 5D; Galli et al., 2010). Furthermore, the expression of *Tbx5*, which is located ~163 kb downstream of *Tbx3* as part of the same gene cluster, is not affected in *Hand2*-deficient forelimb buds (Figure S6B). Several HAND2 ChIP peaks were also detected in the *Tbx2-Tbx4* genomic landscape (Figures S6C and S6D). Similar to the *Tbx3-Tbx5* genomic landscape, *Tbx2*, but not *Tbx4*, expression is reduced in *Hand2*-deficient limb buds (Figures S6E and S6F). These apparent similarities in *cis*-regulation are likely related to the emergence of these gene clusters by duplication of an ancestral complex (Agulnik et al., 1996). Genetic and overexpression analysis has previously implicated *Tbx3* in early forelimb development, together with *Hand2* and *Gli3* (Davenport et al., 2003; Rallis et al., 2005), whereas *Tbx2* is essential only during termination of limb bud outgrowth (Farin et al., 2013). Therefore, we focused our analysis on the HAND2-TBX3 interactions during the onset of forelimb bud development. HAND2 and TBX3 proteins are initially coexpressed (Figure S6G). However, TBX3 becomes rapidly more restricted than HAND2 such that the double-positive cells hallmark the proximal-posterior

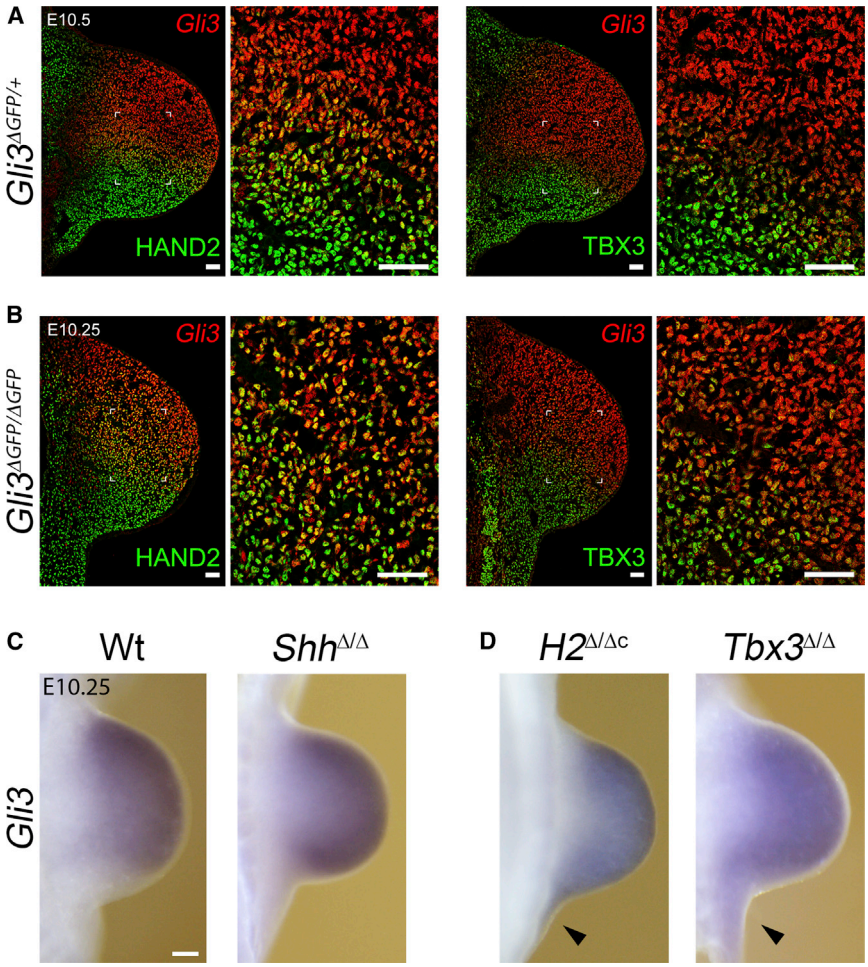

Figure 6. The TBX3 Transcriptional Repressor Participates in Excluding *Gli3* from the Posterior Limb Bud Mesenchyme

(A and B) Left: colocalization of HAND2^{3xF} proteins (green) with *Gli3* transcripts (red) in *Gli3*$^{\Delta GFP/+}$ (E10.5, 35–36 somites) and *Gli3*-deficient (*Gli3*$^{\Delta GFP/\Delta GFP}$; E10.25, 32–33 somites) forelimb buds. Right: colocalization of TBX3 proteins (green) with *Gli3* transcripts (red) in forelimb buds of the same genotypes. White marks indicate the enlargements. Cells coexpressing HAND2^{3xF} or TBX3 proteins with *Gli3* transcripts appear yellow. Scale bar, 50 μm.

(C and D) *Gli3* expression in wild-type, *Shh*-deficient, *Hand2*$^{\Delta/\Delta c}$, and *Tbx3*$^{\Delta/\Delta}$ forelimb buds (E10.25; 32–33 somites). Arrowheads point to expanded *Gli3* expression in the posterior flank mesenchyme. Scale bar, 100 μm.

See also Figure S7.

forelimb bud and posterior flank (Figure 5E). In *Shh*-deficient forelimb buds, both protein domains are more restricted but are otherwise maintained (right panels, Figure 5E). In contrast, TBX3 is absent from *Hand2*$^{\Delta/\Delta c}$ and *Hand2*$^{\Delta/\Delta c}$*Gli3*$^{\Delta/\Delta}$ forelimb buds, with the exception of few positive cells at the proximal border (right panels, Figure 5F). Taken together, these results provide compelling evidence that *Tbx3* is a direct transcriptional target of HAND2 in the posterior and flank mesenchyme during the onset of limb bud development.

To gain insight into the potential involvement of TBX3 in AP patterning of the early limb bud mesenchyme, the spatial distribution of the mesenchymal cells actively transcribing *Gli3* was determined in relation to HAND2 and TBX3 proteins (Figures 6A and 6B). To achieve cellular resolution, the *Gli3* allele expressing EGFP under control of the endogenous locus (Lopez-Rios et al., 2012) was used in combination with GFP antibodies (red fluorescence; Figures 6A and 6B). While the GLI3R and HAND2 protein domains are increasingly separated (Figure 4B), a significant fraction of boundary cells continue to coexpress HAND2 protein and *Gli3* transcripts in wild-type limb buds (yellow fluorescence, left panels, Figure 6A). In contrast, far fewer cells coexpress TBX3 and *Gli3* in the boundary region (right panels, Figure 6A). This difference is even more striking in *Gli3*$^{\Delta/\Delta}$ forelimb buds, which continue to express the mutant *Gli3* transcripts (Figure 6B). There is a large population of cells coexpressing HAND2 and *Gli3* due to the anterior expansion of the *Hand2* expression domain in *Gli3*-deficient limb buds (left panels, Figure 6B; te Welscher et al., 2002). However, TBX3 remains posteriorly restricted in *Gli3*-deficient limb buds, and similar to wild-types, only few cells coexpress TBX3 proteins and *Gli3* transcripts (right panels, Figure 6B). This boundary is also retained in *Shh*-deficient forelimb buds in spite of the posterior expansion of *Gli3* (Figures S7A and S7B). These results show that HAND2 is not sufficient to establish a sharp boundary but rather that TBX3 defines the limit between the anterior *Gli3*-positive and posterior *Gli3*-negative mesenchymal cells. Indeed, the comparative analysis of wild-type, *Shh*-deficient, and *Tbx3*-deficient forelimb buds reveals that *Tbx3* is required to establish this boundary (Figures 6C and 6D). In *Shh*-deficient limb buds, *Gli3* transcription expands posteriorly with more restricted HAND2 and TBX3 domains but fails to reach the posterior margin (right panel, Figures 6C, 5E, and S7A). Rather strikingly, *Gli3* expression expands into the posterior flank mesenchyme in *Tbx3*-deficient forelimb buds as in *Hand2*-deficient limb buds (Figure 6D). *Hand2*-deficient forelimb buds lack *Tbx3* (Figures 5D and 5F) in their posterior mesenchyme, whereas *Hand2* transcripts remain in *Tbx3*-deficient limb buds albeit at reduced levels (Figure S7C). Together, these results corroborate the proposal that the HAND2 transcriptional target *Tbx3* is required to establish the posterior *Gli3* expression boundary by inhibiting its expression in the posterior-most mesenchyme (Figures 6 and 7).

DISCUSSION

There is ample evidence that tissue-specific CRMs orchestrate the dynamics of gene expression during embryonic development and fine-tune morphogenesis as a consequence of their

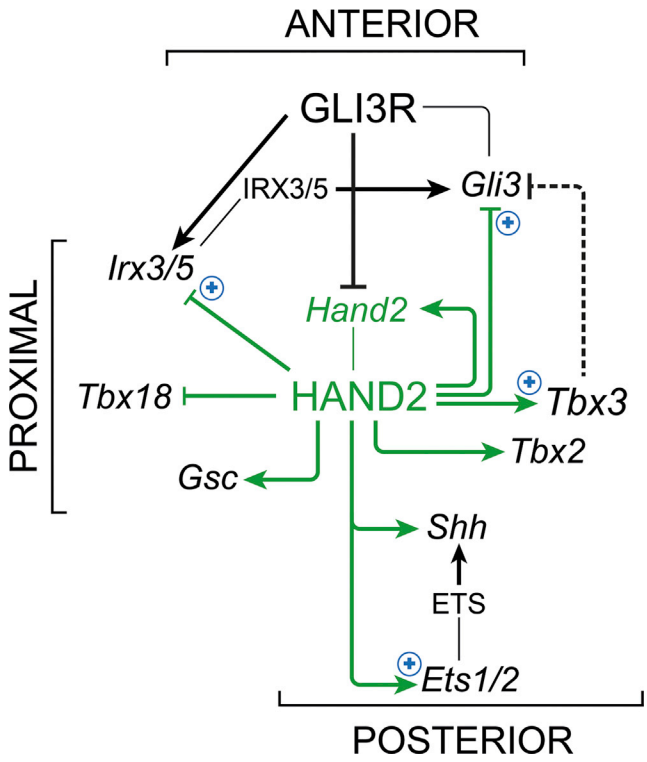

Figure 7. The Major Transcriptional Interactions and Networks Governed by HAND2 in the Forelimb Bud Mesenchyme Upstream of SHH

HAND2 is at the core of the transcriptional networks that control establishment of a proximal, anterior, and posterior compartment in early forelimb buds. In addition to directly impacting on *Shh* and *Gli3* expression, HAND2 re-enforces their activation and repression via *Ets1/2* and *Tbx3*, respectively. Solid lines indicate direct interactions, whereas dashed lines indicate interactions deduced from genetic analysis. Note that the activating or repressive nature of the interactions has mostly been deduced from genetic analysis. (+) indicates CRMs interacting with HAND2 chromatin complexes that have been identified in this study and drive *LacZ* reporter expression in the forelimb bud mesenchyme.

often highly dynamic regulation (Attanasio et al., 2013; Spitz and Furlong, 2012). Functional modification of CRMs in an increasing number of genomic landscapes has been causally linked to both adaptive evolution and human congenital malformations (Anderson et al., 2012; Lopez-Rios et al., 2014). Therefore, it is important to identify the *trans*-acting factors and complexes that regulate these CRMs in a tissue and stage-specific manner. To this aim, we have inserted a 3xFLAG-tag into the endogenous HAND2 protein, which permitted us to uncover genomic regions enriched in HAND2-containing chromatin complexes in mouse embryos. The current study focuses on an in-depth functional analysis of HAND2-CRMs in genomic landscapes of transcriptional regulators that are required during early mouse forelimb bud development. This analysis uncovers the architecture of a network of HAND2 target transcription factors that function in early determinative events that set up the proximal, anterior, and posterior domains during the onset of forelimb bud outgrowth (Figure 7). An essential role of HAND2 in proximal skeletal development was revealed by the fact that its early *Hoxb6*-Cre mediated conditional inactivation disrupts scapular head morphogenesis. Our study provides good evidence that this is a consequence of HAND2 directly regulating the expression of transcription factors that function in the development of the proximal limb skeletal elements, such as *Gsc*, *Irx3*, *Irx5*, and *Tbx18* (Figure 7). In particular, the HAND2 ChIP analysis identifies a CRM located upstream of *Irx3* that is active in the limb bud mesenchyme. In turn, IRX3 regulates *Gli3* expression by directly interacting with a limb bud mesenchymal CRM located in the *Gli3* genomic landscape (Abbasi et al., 2010; Li et al., 2014). These direct interactions begin to reveal the underlying complexity of the *cis*-regulatory circuitry operating during the onset of limb bud development (Figure 7). In summary, our genetic analysis supports the proposal that the HAND2-regulated gene networks are required to pattern the early mesenchymal territory that gives rise to the proximal limb skeletal elements in a *Shh*-independent manner (Ahn and Joyner, 2004; Chiang et al., 2001).

It is unclear at which stage AP axis polarity is established in mouse limb buds, but Tanaka et al. (2000) showed that the competence to activate *Shh* expression is widespread and without posterior bias in the forelimb field of early mouse embryos (E9.0). Together with other studies (see Introduction), this suggests that the limb bud mesenchyme might only be polarized along the AP axis during the onset of limb bud development in mouse embryos. The present study shows that the nuclear HAND2 and GLI3R proteins are initially coexpressed by the mesenchymal progenitors that give rise to the forelimb bud. However, during initiation of limb bud development, the spatial distributions of the two transcriptional regulators rapidly segregate into a distinct GLI3R-positive anterior and HAND2-positive posterior compartment. In addition to establishing this dynamic segregation with cellular resolution, we identify the HAND2-dependent *cis*-regulatory interactions and transcription factor networks that establish these anterior and posterior compartments (Figure 7). The loss of *Hand2* transcripts and proteins from the anterior limb bud mesenchyme (te Welscher et al., 2002; this study) is the result of GLI3R-mediated direct repression (Vokes et al., 2008). The HAND2 ChIP analysis identifies one CRM in the *Gli3* genomic landscape that is active in limb buds, with exception of the most posterior mesenchyme. The transcriptional regulation of *Gli3* in early limb buds is complex and likely controlled by several CRMs with similar activities, one of which is bound by IRX3, a direct transcriptional target of *Hand2* (Abbasi et al., 2010; Li et al., 2014; Visel et al., 2007; this study). While the genetic analysis shows that *Hand2* is required to repress the expression of *Gli3* and other direct targets in the posterior mesenchyme, our transgenic studies of HAND2-interacting CRMs rather reveals their ability to activate *LacZ* expression in the limb bud mesenchyme. HAND2 was first described as a transcriptional activator (Dai and Cserjesi, 2002), but more recently its transcriptional repressing activity has been established in the context of its interaction with a specific CRM that regulates the *Dlx5/6* gene cluster (Barron et al., 2011). Furthermore, HAND2 forms heterodimers with transcriptional repressors, such as TWIST1 and RUNX2 (Firulli et al., 2005; Funato et al., 2009), which could determine the repressive activity of HAND2 chromatin complexes interacting with CRMs in, e.g., the *Gli3* genomic landscape. Alternatively, the repressive

effect of HAND2 on *Gli3* could be mediated via the transcriptional target *Tbx3*, which is required to repress *Gli3* in the posterior mesenchyme. In fact, TBX3 has an essential role in positioning the *Gli3* expression boundary (Figure 7), and its overexpression in forelimb buds of chicken embryos inhibits *Gli3* expression (Rallis et al., 2005). Finally, HAND2 controls the activation of *Shh* expression by directly binding to the ZRS and indirectly via its transcriptional targets *Ets1* and *Ets2* that also regulate *Shh* (Lettice et al., 2012, 2014). Such feed-forward loops are important motifs within transcriptional networks as they contribute to their stability and robustness (Alon, 2007).

Previous studies had provided genetic and experimental evidence that both proximodistal and AP identities are specified early during limb bud development (Dudley et al., 2002; Zhu et al., 2008). Our study now uncovers distinct transcriptional networks interlinked by HAND2 that are required to set-up the initial proximal, posterior, and anterior mesenchymal compartments prior to the onset of SHH signaling. These networks define proximal fates and the AP boundaries with cellular precision through selective activation and/or repression of downstream transcriptional regulators. The direct cross-regulation among these transcriptional regulators not only defines the limb bud mesenchymal compartments but also enables activation of SHH signaling, which then elaborates these compartments during distal progression of limb bud outgrowth.

EXPERIMENTAL PROCEDURES

For generation of the *Hand2*^{3xF} allele and details on methodology, see the Supplemental Experimental Procedures.

Mouse Strains and Embryos

Experiments involving mice were performed with strict adherence to Swiss law, the 3R principles, and the Basel Declaration. All animal studies were approved by the cantonal animal welfare and ethics committees. The procedures for generating transgenic mice at the Lawrence Berkeley National Laboratory (LBNL) were reviewed and approved by the LBNL Animal Welfare and Research Committee. The *Hand2*^{3xF} and *Gli3*^{C3xF} alleles were maintained in an NMRI background. The *Hand2*^{f} (floxed), *Hand2*$^{\Delta}$, and *Gli3*$^{\Delta GFP}$ alleles were maintained in mixed backgrounds. The *Gli3*^{C3xF} allele was constructed by inserting a 3XFLAG epitope tag in frame at the carboxy terminus of the endogenous GLI3 protein. Western blotting detects the 190 kD full-length GLI3 protein. Mice and embryos homozygous for this allele are phenotypically wild-type and will be described elsewhere (J.L.-R. and R.Z., unpublished data). The *Shh*^{GFPCre} allele (Harfe et al., 2004) and the *Hoxb6-Cre* transgene (Lowe et al., 2000) were maintained in a C57BL/6J background. The *Tbx3*^{Venus} allele used to generate *Tbx3*-deficient embryos recapitulates all known *Tbx3* loss-of-function phenotypes and will be described elsewhere (R.M. and V.M.C., unpublished data).

Immunofluorescence

Limb buds were fixed in 4% paraformaldehyde for 2–3 hr at 4°C, and proteins were detected on 10 μm cryosections. Primary antibodies against the FLAG epitope (M2; 1:500; Sigma), GLI3 (3.6 ng/ml; clone 6F5; Wen et al., 2010), TBX3 (1:300; E-20; Santa Cruz), and GFP (1:1,000; Life Technologies) were used. Goat anti-mouse (FLAG/GLI3), goat anti-rabbit (GFP), and rabbit/donkey anti-goat (TBX3) secondary antibodies conjugated to Alexa Fluor 488 or 594 (1:1,000; Life Technologies) were used for detection. For colocalization of HAND2 and GLI3R, anti-FLAG (M2; F3165, Sigma) antibodies were labeled with Alexa Fluor 488 using the APEX antibody labeling kit (Life Technologies). Sequential treatment with rabbit anti-Alexa Fluor 488 (Life Technologies) and goat anti-rabbit 488 Alexa Fluor enhanced the signal. Nuclei were counterstained with Hoechst-33258. The *Shh*^{GFPCre} and *Gli3*$^{\Delta GFP}$ null alleles were used in combination with immunodetection of GFP to visualize cells expressing *Shh* or *Gli3*, respectively. Autofluorescence, e.g., of blood cells, was detected equally in all channels. Therefore, it was captured utilizing the 633 nm laser of the confocal microscope and digitally removed using the subtraction mode in Photoshop CS5 (Adobe) as shown in Figure S1A. Images were acquired using a Leica SP5 confocal microscope.

ChIP-qPCR and ChIP-Seq Analysis

Fore- and hindlimb buds dissected from ~50 *Hand2*$^{3xF/3xF}$ embryos at E10.5 were processed for ChIP as described (Lopez-Rios et al., 2012; Vokes et al., 2008) using M2 anti-FLAG antibody (F1804; Sigma). For time course experiments, 20 fore- and hindlimbs of E11.5 or E12.5 *Hand2*$^{3xF/3xF}$ embryos were processed in an identical manner. Chromatin was fragmented for 15 (E10.5) or 20 min (E11.5, E12.5) using a S220 Covaris Ultrasonicator, which yielded average fragment sizes in the range of 200–300 bp. All results (mean ± SD) represent three independent biological replicates. The details of the ChIP-seq analysis are given in the Supplemental Experimental Procedures.

ACCESSION NUMBERS

The GEO database accession number for all data sets reported in this paper is GSE55707.

SUPPLEMENTAL INFORMATION

Supplemental Information includes Supplemental Experimental Procedures, seven figures and five tables and can be found with this article online at http://dx.doi.org/10.1016/j.devcel.2014.09.018.

ACKNOWLEDGMENTS

We wish to thank the mouse transgenic core facility of the University of Basel for generation of chimeric mice and A. Offinger and her team for excellent animal care. Frédéric Laurent is thanked for performing the OPT analysis. We are grateful to Jennifer Akiyama for generation of constructs, Ina Nissen (D-BSSE) for the preparation of the ChIP-seq library, and Isabelle Ginez for preparing the tissue sections. This research was supported by Swiss National Science Foundation grants (31003A_130803/146248) and both cantons of Basel (to R.Z.), an EU Reintegration grant (PERG-GA-2009-246576 to J.L.-R.), a Netherlands Heart Foundation grant (2010B205) (to V.M.C.), and NIH grants (R01HG003988 and U01DE020060) (to A.V.). A.V.'s research was conducted at the E.O. Lawrence Berkeley National Laboratory and performed under a Department of Energy Contract (DE-AC02-05CH11231), University of California. X.W. and S.J.S. are employees of Genentech, a member of the Roche group.

Received: March 15, 2014
Revised: August 29, 2014
Accepted: September 29, 2014
Published: November 10, 2014

REFERENCES

Abbasi, A.A., Paparidis, Z., Malik, S., Bangs, F., Schmidt, A., Koch, S., Lopez-Rios, J., and Grzeschik, K.H. (2010). Human intronic enhancers control distinct sub-domains of Gli3 expression during mouse CNS and limb development. BMC Dev. Biol. *10*, 44.

Agulnik, S.I., Garvey, N., Hancock, S., Ruvinsky, I., Chapman, D.L., Agulnik, I., Bollag, R., Papaioannou, V., and Silver, L.M. (1996). Evolution of mouse T-box genes by tandem duplication and cluster dispersion. Genetics *144*, 249–254.

Ahn, S., and Joyner, A.L. (2004). Dynamic changes in the response of cells to positive hedgehog signaling during mouse limb patterning. Cell *118*, 505–516.

Alon, U. (2007). Network motifs: theory and experimental approaches. Nat. Rev. Genet. *8*, 450–461.

Anderson, E., Peluso, S., Lettice, L.A., and Hill, R.E. (2012). Human limb abnormalities caused by disruption of hedgehog signaling. Trends Genet. *28*, 364–373.

Attanasio, C., Nord, A.S., Zhu, Y., Blow, M.J., Li, Z., Liberton, D.K., Morrison, H., Plajzer-Frick, I., Holt, A., Hosseini, R., et al. (2013). Fine tuning of craniofacial morphology by distant-acting enhancers. Science *342*, 1241006.

Barron, F., Woods, C., Kuhn, K., Bishop, J., Howard, M.J., and Clouthier, D.E. (2011). Downregulation of Dlx5 and Dlx6 expression by Hand2 is essential for initiation of tongue morphogenesis. Development *138*, 2249–2259.

Belo, J.A., Leyns, L., Yamada, G., and De Robertis, E.M. (1998). The prechordal midline of the chondrocranium is defective in Goosecoid-1 mouse mutants. Mech. Dev. *72*, 15–25.

Capdevila, J., Tsukui, T., Rodríquez Esteban, C., Zappavigna, V., and Izpisúa Belmonte, J.C. (1999). Control of vertebrate limb outgrowth by the proximal factor Meis2 and distal antagonism of BMPs by Gremlin. Mol. Cell *4*, 839–849.

Capellini, T.D., Di Giacomo, G., Salsi, V., Brendolan, A., Ferretti, E., Srivastava, D., Zappavigna, V., and Selleri, L. (2006). Pbx1/Pbx2 requirement for distal limb patterning is mediated by the hierarchical control of Hox gene spatial distribution and Shh expression. Development *133*, 2263–2273.

Capellini, T.D., Vaccari, G., Ferretti, E., Fantini, S., He, M., Pellegrini, M., Quintana, L., Di Giacomo, G., Sharpe, J., Selleri, L., and Zappavigna, V. (2010). Scapula development is governed by genetic interactions of Pbx1 with its family members and with Emx2 via their cooperative control of Alx1. Development *137*, 2559–2569.

Charité, J., McFadden, D.G., and Olson, E.N. (2000). The bHLH transcription factor dHAND controls *Sonic hedgehog* expression and establishment of the zone of polarizing activity during limb development. Development *127*, 2461–2470.

Chiang, C., Litingtung, Y., Harris, M.P., Simandl, B.K., Li, Y., Beachy, P.A., and Fallon, J.F. (2001). Manifestation of the limb prepattern: limb development in the absence of sonic hedgehog function. Dev. Biol. *236*, 421–435.

Cotney, J., Leng, J., Oh, S., DeMare, L.E., Reilly, S.K., Gerstein, M.B., and Noonan, J.P. (2012). Chromatin state signatures associated with tissue-specific gene expression and enhancer activity in the embryonic limb. Genome Res. *22*, 1069–1080.

Dai, Y.S., and Cserjesi, P. (2002). The basic helix-loop-helix factor, HAND2, functions as a transcriptional activator by binding to E-boxes as a heterodimer. J. Biol. Chem. *277*, 12604–12612.

Davenport, T.G., Jerome-Majewska, L.A., and Papaioannou, V.E. (2003). Mammary gland, limb and yolk sac defects in mice lacking Tbx3, the gene mutated in human ulnar mammary syndrome. Development *130*, 2263–2273.

Dudley, A.T., Ros, M.A., and Tabin, C.J. (2002). A re-examination of proximodistal patterning during vertebrate limb development. Nature *418*, 539–544.

Farin, H. (2009). Function and regulation of the murine T-box genes Tbx15 and Tbx18. PhD thesis (Hannover: University of Hannover).

Farin, H.F., Lüdtke, T.H., Schmidt, M.K., Placzko, S., Schuster-Gossler, K., Petry, M., Christoffels, V.M., and Kispert, A. (2013). Tbx2 terminates shh/fgf signaling in the developing mouse limb bud by direct repression of gremlin1. PLoS Genet. *9*, e1003467.

Firulli, B.A., Krawchuk, D., Centonze, V.E., Vargesson, N., Virshup, D.M., Conway, S.J., Cserjesi, P., Laufer, E., and Firulli, A.B. (2005). Altered Twist1 and Hand2 dimerization is associated with Saethre-Chotzen syndrome and limb abnormalities. Nat. Genet. *37*, 373–381.

Funato, N., Chapman, S.L., McKee, M.D., Funato, H., Morris, J.A., Shelton, J.M., Richardson, J.A., and Yanagisawa, H. (2009). Hand2 controls osteoblast differentiation in the branchial arch by inhibiting DNA binding of Runx2. Development *136*, 615–625.

Galli, A., Robay, D., Osterwalder, M., Bao, X., Bénazet, J.D., Tariq, M., Paro, R., Mackem, S., and Zeller, R. (2010). Distinct roles of Hand2 in initiating polarity and posterior Shh expression during the onset of mouse limb bud development. PLoS Genet. *6*, e1000901.

Harfe, B.D., Scherz, P.J., Nissim, S., Tian, H., McMahon, A.P., and Tabin, C.J. (2004). Evidence for an expansion-based temporal Shh gradient in specifying vertebrate digit identities. Cell *118*, 517–528.

Horsthuis, T., Buermans, H.P., Brons, J.F., Verkerk, A.O., Bakker, M.L., Wakker, V., Clout, D.E., Moorman, A.F., 't Hoen, P.A., and Christoffels, V.M. (2009). Gene expression profiling of the forming atrioventricular node using a novel tbx3-based node-specific transgenic reporter. Circ. Res. *105*, 61–69.

Kmita, M., Tarchini, B., Zàkàny, J., Logan, M., Tabin, C.J., and Duboule, D. (2005). Early developmental arrest of mammalian limbs lacking HoxA/HoxD gene function. Nature *435*, 1113–1116.

Kozhemyakina, E., Ionescu, A., and Lassar, A.B. (2014). GATA6 is a crucial regulator of Shh in the limb bud. PLoS Genet. *10*, e1004072.

Lettice, L.A., Heaney, S.J., Purdie, L.A., Li, L., de Beer, P., Oostra, B.A., Goode, D., Elgar, G., Hill, R.E., and de Graaff, E. (2003). A long-range Shh enhancer regulates expression in the developing limb and fin and is associated with preaxial polydactyly. Hum. Mol. Genet. *12*, 1725–1735.

Lettice, L.A., Williamson, I., Wiltshire, J.H., Peluso, S., Devenney, P.S., Hill, A.E., Essafi, A., Hagman, J., Mort, R., Grimes, G., et al. (2012). Opposing functions of the ETS factor family define Shh spatial expression in limb buds and underlie polydactyly. Dev. Cell *22*, 459–467.

Lettice, L.A., Williamson, I., Devenney, P.S., Kilanowski, F., Dorin, J., and Hill, R.E. (2014). Development of five digits is controlled by a bipartite long-range cis-regulator. Development *141*, 1715–1725.

Li, D., Sakuma, R., Vakili, N.A., Mo, R., Puviindran, V., Deimling, S., Zhang, X., Hopyan, S., and Hui, C.C. (2014). Formation of proximal and anterior limb skeleton requires early function of Irx3 and Irx5 and is negatively regulated by Shh signaling. Dev. Cell *29*, 233–240.

Lopez-Rios, J., Speziale, D., Robay, D., Scotti, M., Osterwalder, M., Nusspaumer, G., Galli, A., Holländer, G.A., Kmita, M., and Zeller, R. (2012). GLI3 constrains digit number by controlling both progenitor proliferation and BMP-dependent exit to chondrogenesis. Dev. Cell *22*, 837–848.

Lopez-Rios, J., Duchesne, A., Speziale, D., Andrey, G., Peterson, K.A., Germann, P., Unal, E., Liu, J., Floriot, S., Barbey, S., et al. (2014). Attenuated sensing of SHH by Ptch1 underlies evolution of bovine limbs. Nature *511*, 46–51.

Lowe, L.A., Yamada, S., and Kuehn, M.R. (2000). HoxB6-Cre transgenic mice express Cre recombinase in extra-embryonic mesoderm, in lateral plate and limb mesoderm and at the midbrain/hindbrain junction. Genesis *26*, 118–120.

Mao, J., McGlinn, E., Huang, P., Tabin, C.J., and McMahon, A.P. (2009). Fgf-dependent Etv4/5 activity is required for posterior restriction of Sonic Hedgehog and promoting outgrowth of the vertebrate limb. Dev. Cell *16*, 600–606.

Mariani, F.V., Ahn, C.P., and Martin, G.R. (2008). Genetic evidence that FGFs have an instructive role in limb proximal-distal patterning. Nature *453*, 401–405.

Mercader, N., Leonardo, E., Piedra, M.E., Martínez-A, C., Ros, M.A., and Torres, M. (2000). Opposing RA and FGF signals control proximodistal vertebrate limb development through regulation of Meis genes. Development *127*, 3961–3970.

Niederreither, K., Vermot, J., Schuhbaur, B., Chambon, P., and Dollé, P. (2002). Embryonic retinoic acid synthesis is required for forelimb growth and anteroposterior patterning in the mouse. Development *129*, 3563–3574.

Osterwalder, M., Galli, A., Rosen, B., Skarnes, W.C., Zeller, R., and Lopez-Rios, J. (2010). Dual RMCE for efficient re-engineering of mouse mutant alleles. Nat. Methods *7*, 893–895.

Rallis, C., Del Buono, J., and Logan, M.P. (2005). Tbx3 can alter limb position along the rostrocaudal axis of the developing embryo. Development *132*, 1961–1970.

Sagai, T., Hosoya, M., Mizushina, Y., Tamura, M., and Shiroishi, T. (2005). Elimination of a long-rangecis-regulatory module causes complete loss of limb-specific Shh expression and truncation of the mouse limb. Development *132*, 797–803.

Selleri, L., Depew, M.J., Jacobs, Y., Chanda, S.K., Tsang, K.Y., Cheah, K.S., Rubenstein, J.L., O'Gorman, S., and Cleary, M.L. (2001). Requirement for Pbx1 in skeletal patterning and programming chondrocyte proliferation and differentiation. Development *128*, 3543–3557.

Spitz, F., and Furlong, E.E. (2012). Transcription factors: from enhancer binding to developmental control. Nat. Rev. Genet. *13*, 613–626.

Srivastava, D., Thomas, T., Lin, Q., Kirby, M.L., Brown, D., and Olson, E.N. (1997). Regulation of cardiac mesodermal and neural crest development by the bHLH transcription factor, dHAND. Nat. Genet. *16*, 154–160.

Tanaka, M., Cohn, M.J., Ashby, P., Davey, M., Martin, P., and Tickle, C. (2000). Distribution of polarizing activity and potential for limb formation in mouse and chick embryos and possible relationships to polydactyly. Development *127*, 4011–4021.

te Welscher, P., Fernandez-Teran, M., Ros, M.A., and Zeller, R. (2002). Mutual genetic antagonism involving GLI3 and dHAND prepatterns the vertebrate limb bud mesenchyme prior to SHH signaling. Genes Dev. *16*, 421–426.

Vincentz, J.W., Barnes, R.M., and Firulli, A.B. (2011). Hand factors as regulators of cardiac morphogenesis and implications for congenital heart defects. Birth Defects Res. A. Clin. Mol. Terat. *91*, 485–494.

Visel, A., Minovitsky, S., Dubchak, I., and Pennacchio, L.A. (2007). VISTA Enhancer Browser—a database of tissue-specific human enhancers. Nucleic Acids Res. *35*, D88–D92.

Vitobello, A., Ferretti, E., Lampe, X., Vilain, N., Ducret, S., Ori, M., Spetz, J.F., Selleri, L., and Rijli, F.M. (2011). Hox and Pbx factors control retinoic acid synthesis during hindbrain segmentation. Dev. Cell *20*, 469–482.

Vokes, S.A., Ji, H., Wong, W.H., and McMahon, A.P. (2008). A genome-scale analysis of thecis-regulatory circuitry underlying sonic hedgehog-mediated patterning of the mammalian limb. Genes Dev. *22*, 2651–2663.

Wang, B., Fallon, J.F., and Beachy, P.A. (2000). Hedgehog-regulated processing of Gli3 produces an anterior/posterior repressor gradient in the developing vertebrate limb. Cell *100*, 423–434.

Wen, X., Lai, C.K., Evangelista, M., Hongo, J.A., de Sauvage, F.J., and Scales, S.J. (2010). Kinetics of hedgehog-dependent full-length Gli3 accumulation in primary cilia and subsequent degradation. Mol. Cell. Biol. *30*, 1910–1922.

Zeller, R., López-Ríos, J., and Zuniga, A. (2009). Vertebrate limb bud development: moving towards integrative analysis of organogenesis. Nat. Rev. Genet. *10*, 845–858.

Zhang, Z., Verheyden, J.M., Hassell, J.A., and Sun, X. (2009). FGF-regulated Etv genes are essential for repressing Shh expression in mouse limb buds. Dev. Cell *16*, 607–613.

Zhang, Z., Sui, P., Dong, A., Hassell, J., Cserjesi, P., Chen, Y.T., Behringer, R.R., and Sun, X. (2010). Preaxial polydactyly: interactions among ETV, TWIST1 and HAND2 control anterior-posterior patterning of the limb. Development *137*, 3417–3426.

Zhao, X., Sirbu, I.O., Mic, F.A., Molotkova, N., Molotkov, A., Kumar, S., and Duester, G. (2009). Retinoic acid promotes limb induction through effects on body axis extension but is unnecessary for limb patterning. Curr. Biol. *19*, 1050–1057.

Zhu, J., Nakamura, E., Nguyen, M.T., Bao, X., Akiyama, H., and Mackem, S. (2008). Uncoupling Sonic hedgehog control of pattern and expansion of the developing limb bud. Dev. Cell *14*, 624–632.

Developmental Cell, Volume *31*

Supplemental Information

HAND2 Targets Define a Network of Transcriptional Regulators that Compartmentalize the Early Limb Bud Mesenchyme

Marco Osterwalder, Dario Speziale, Malak Shoukry, Rajiv Mohan, Robert Ivanek, Manuel Kohler, Christian Beisel, Xiaohui Wen, Suzie J. Scales, Vincent M. Christoffels, Axel Visel, Javier Lopez-Rios, and Rolf Zeller

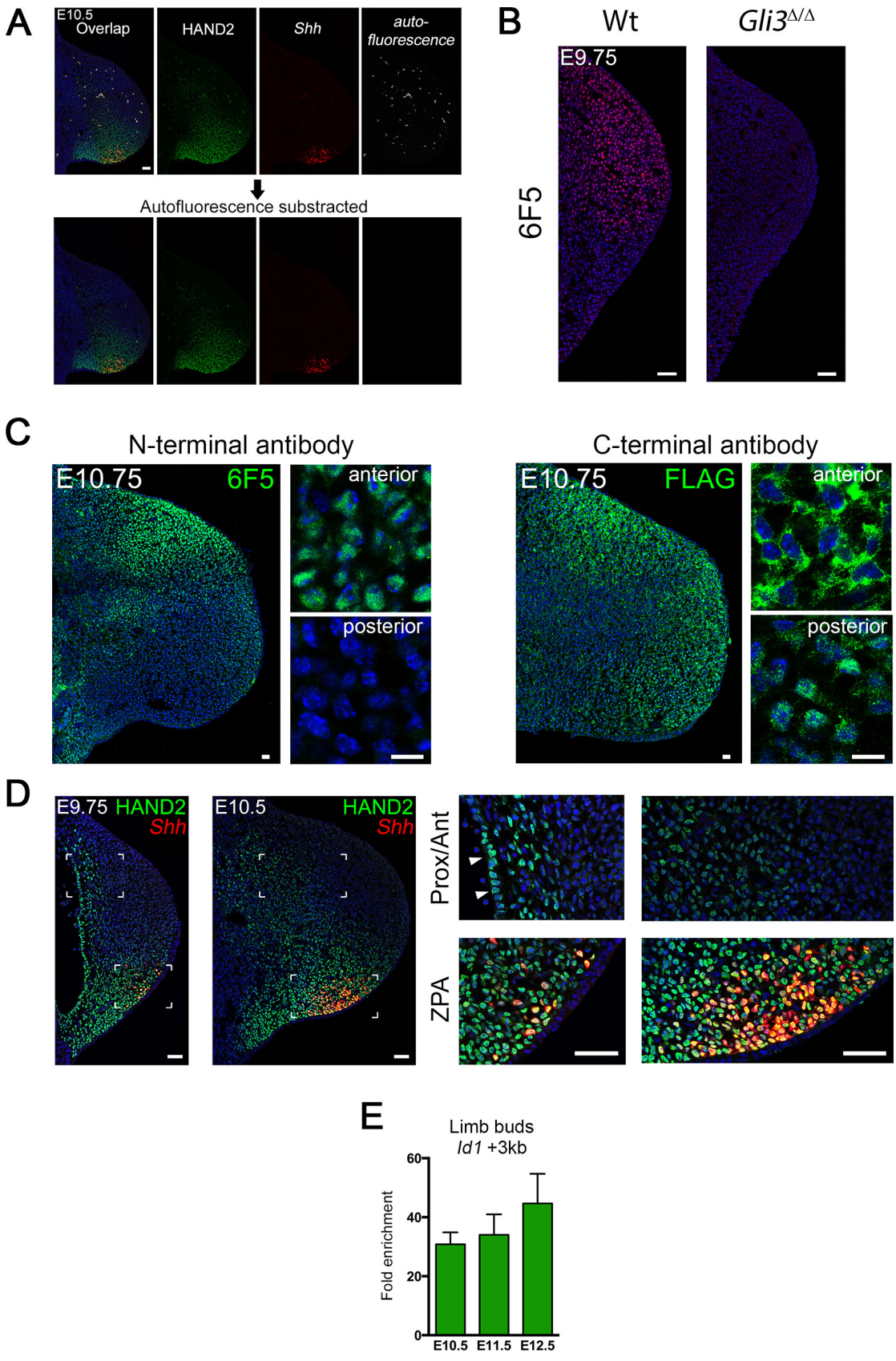
A
E10.5
Overlap
HAND2
Shh
auto-
fluorescence
Autofluorescence substracted
B
Wt
Gli3Δ/Δ
E9.75
6F5
C
N-terminal antibody
C-terminal antibody
E10.75
6F5
anterior
posterior
E10.75
FLAG
anterior
posterior
D
E9.75 HAND2
Shh
E10.5
HAND2
Shh
Prox/Ant
ZPA
E
Limb buds
Id1 +3kb
Fold enrichment
60
40
20
0
E10.5
E11.5
E12.5

Figure S1 (related to Figure 1). Immunofluorescence analysis to study the HAND2, GLI3R and GLI3A proteins in mouse forelimb buds.

(A) Subtraction of auto-fluorescent hematopoietic and vascular cells from immunofluorescent images of limb bud sections. Autofluorescence was captured using a separate confocal channel (white, excitation 633nm) and digitally removed using the subtraction mode in Photoshop CS5 (Adobe). Nuclei appear blue due to Hoechst-33258 counterstaining. Scale bars: 50μm.

(B) The 6F5 monoclonal anti-GLI3 antibody (raised against the N-terminal part of the GLI3 protein, Wen et al., 2010) detects nuclear GLI3 proteins (red fluorescence) specifically in the anterior mesenchyme of forelimb buds at E9.75 (28-29 somites). No fluorescence is detected in *Gli3*-deficient limb buds, which establishes the specificity of the antibodies for GLI3 proteins.

(C) Left panels: the 6F5 antibody (Wen et al., 2010) detects predominantly the nuclear GLI3R isoform by immunofluorescence in limb buds. As in early limb buds (panel B), the 6F5 antibody detects nuclear GLI3 proteins only in the anterior limb bud mesenchyme, corresponding to the GLI3R isoform, during SHH-dependent limb bud outgrowth (E10.75). In contrast, no immunofluorescence is detected in the posterior mesenchyme, which upon exposure to SHH should accumulate the full-length nuclear isoform corresponding to the GLI3 activator (GLI3A). Right panels: insertion of a 3xFLAG epitope-tag into the carboxy-terminal end of the endogenous *Gli3* coding region (*Gli3*^{C3xF} allele, see Experimental Procedures) allows specific detection of the full-length GLI3 and GLI3A, but not GLI3R protein isoforms. At E10.75, anti-FLAG antibodies detect nuclear full-length GLI3 proteins, corresponding to the GLI3A isoform, only in the posterior limb bud

mesenchyme. In the anterior mesenchyme of $Gli3^{C3xF/C3xF}$ limb buds, only cytoplasmic full-length GLI3 proteins are detected (i.e. no nuclear GLI3A is present in the anterior margin). Together, the non-overlapping immunofluorescence patterns of the 6F5 and FLAG antibodies show that the 6F5 antibody must only detect the nuclear GLI3R isoform in the anterior limb bud mesenchyme. Scale bars: 25μm.

(D) Co-localization of $HAND2^{3xF}$ (green) and *Shh*-expressing cells (red) in wild-type limb buds (E9.75 and E10.5, yellow indicates co-localization). Rectangles indicate the position of enlargements in proximal-anterior (Prox/Ant) and polarizing (ZPA) regions. The observed pattern of *Shh*-positive and negative cells within the posterior HAND2 domain is consistent with previous observations (Amano et al., 2009). White arrowheads: $HAND2^{3xF}$-positive cells in the mesothelium.

(E) To ensure that the progressive reduction in binding of HAND2 chromatin complexes to the ZRS and other CRMs analyzed by ChIP-qPCR is real, a candidate CRM located ~3kb downstream of the *Id1* transcriptional start site (identified by ChIP-Seq analysis) was used as a control. In contrast to many other regions, the enrichment of *Id1* +3kb region by HAND2 ChIP-qPCR is increased rather than reduced during progression of limb bud development (E10.5 - E12.5).

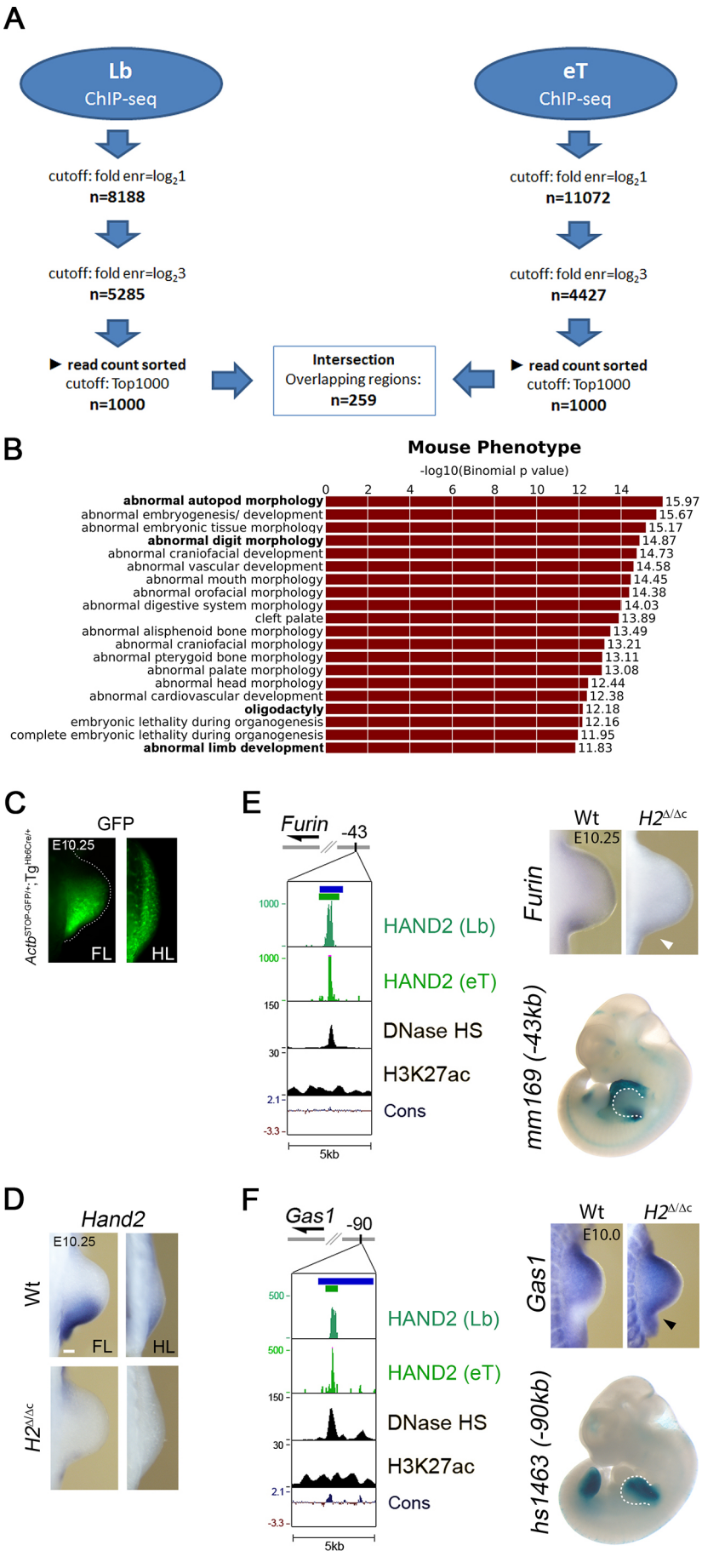
A
Lb
ChIP-seq
eT
ChIP-seq
cutoff: fold enr=log2 1
n=8188
cutoff: fold enr=log2 1
n=11072
cutoff: fold enr=log2 3
n=5285
cutoff: fold enr=log2 3
n=4427
read count sorted
cutoff: Top1000
n=1000
Intersection
Overlapping regions:
n=259
read count sorted
cutoff: Top1000
n=1000
B
Mouse Phenotype
-log10(Binomial p value)
0 2 4 6 8 10 12 14
abnormal autopod morphology 15.97
abnormal embryogenesis/ development 15.67
abnormal embryonic tissue morphology 15.17
abnormal digit morphology 14.87
abnormal craniofacial development 14.73
abnormal vascular development 14.58
abnormal mouth morphology 14.45
abnormal orofacial morphology 14.38
abnormal digestive system morphology 14.03
cleft palate 13.89
abnormal alisphenoid bone morphology 13.49
abnormal craniofacial morphology 13.21
abnormal pterygoid bone morphology 13.11
abnormal palate morphology 13.08
abnormal head morphology 12.44
abnormal cardiovascular development 12.38
oligodactyly 12.18
embryonic lethality during organogenesis 12.16
complete embryonic lethality during organogenesis 11.95
abnormal limb development 11.83
C
GFP
E10.25
FL
HL
Actb STOP-GFP/+; Tg Hsb8Cre/+
D
Hand2
E10.25
Wt
FL
HL
H2 Δ/Δc
E
Furin
-43
1000
1000
150
30
2.1
-3.3
HAND2 (Lb)
HAND2 (eT)
DNase HS
H3K27ac
Cons
5kb
Wt
H2 Δ/Δc
E10.25
Furin
mm169 (-43kb)
F
Gas1
-90
500
500
150
30
2.1
-3.3
HAND2 (Lb)
HAND2 (eT)
DNase HS
H3K27ac
Cons
5kb
Wt
H2 Δ/Δc
E10.0
Gas1
hs1463 (-90kb)

Figure S2 (related to Figure 2). HAND2 binds to tissue specific enhancers and putative CRMs in proximity to genes involved in limb bud development.

(A) Scheme to intersect the limb bud (Lb) and expressing tissues (eT) ChIP-Seq datasets with the aim to identify HAND2 binding regions enriched in both. An overlap of 259 genomic regions enriched in both datasets was identified.

(B) Mouse phenotypes associated with the genes neighboring the 259 genomic regions enriched in both datasets as revealed by GREAT analysis (McLean et al., 2010).

(C) Conditional activation of GFP using the *Actb*$^{STOP\text{-}GFP/+}$ reporter transgene reveals the *Hoxb6Cre* activity in fore- and hindlimb buds at E10.25 (32-33 somites).

(D) Clearance of *Hand2* transcripts from *Hoxb6Cre*$^{tg/+}$ *Hand2*$^{\Delta/\Delta c}$ fore- and hindlimb buds at E10.25 (32-33 somites).

(E, F) Left panels: HAND2 ChIP-Seq profiles for two highly enriched putative CRMs associated with *Furin* (E) and *Gas1* genes (F). For both these putative CRMs the activity has been determined as part of the Vista Enhancer Project. The distance to the corresponding transcriptional start site is indicated in kb. Right panels: expression of these HAND2 target genes in wild-type and *Hand2*$^{\Delta/\Delta c}$ forelimb buds at E10.0-E10.25. In *Hand2*-deficient limb buds, *Furin* is downregulated, while *Gas1* expression expands posteriorly. These two CRMs are able to activate the expression of a *LacZ* reporter transgene in limb bud domains mimicking the endogenous transcript distributions. In the case of *Gas1*, the region assayed for enhancer potential was the human orthologue.

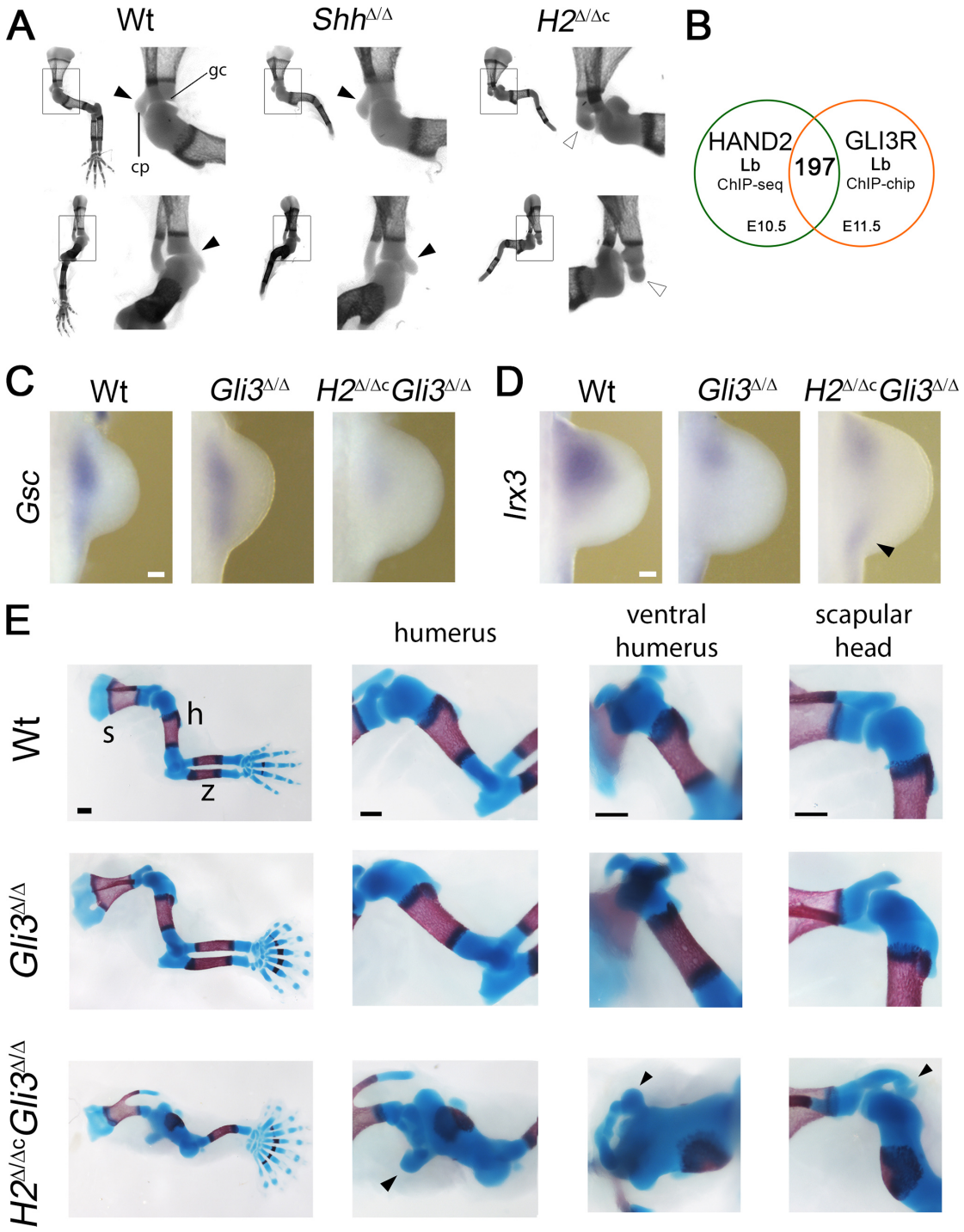

Figure S3 (related to Figure 3). Molecular and morphological defects in *Hand2*$^{\Delta/\Delta c}$*Gli3*$^{\Delta/\Delta}$ forelimb buds generated using the *Hoxb6-Cre* transgene.

(A) Optical Projection Tomography images of wild-type (*Hand2*$^{\Delta c/+}$), *Hand2*$^{\Delta/\Delta c}$ and *Shh*-deficient (*Shh*$^{\Delta/\Delta}$) forelimb skeletons at E16.5. Black arrowheads:

intact articulation of the distal scapula with the head of the humerus. Open arrowheads: malformed and displaced distal scapular structures. gc: glenoid cavity; cp: coracoid process.

(B) Intersection of the top 1000 HAND2 and GLI3R (Vokes et al., 2008) genomic target regions in embryonic limb buds.

(C, D) *Gsc* and *Irx3* expression in wild-type, $Gli3^{\Delta/\Delta}$ and $Hand2^{\Delta/\Delta c}Gli3^{\Delta/\Delta}$ forelimb buds at E10.0 (30-31 somites). Black arrowhead: ectopic *Irx3* expression in the proximal-posterior limb bud mesenchyme. Scale bars: 100μm.

(E) Skeletal preparations of $Hand2^{\Delta/\Delta c}Gli3^{\Delta/\Delta}$ forelimbs at E16.5. Black arrowheads indicate aberrant cartilage structures in the ventral-proximal part of the dysplastic humerus. Scale bars: 500μm.

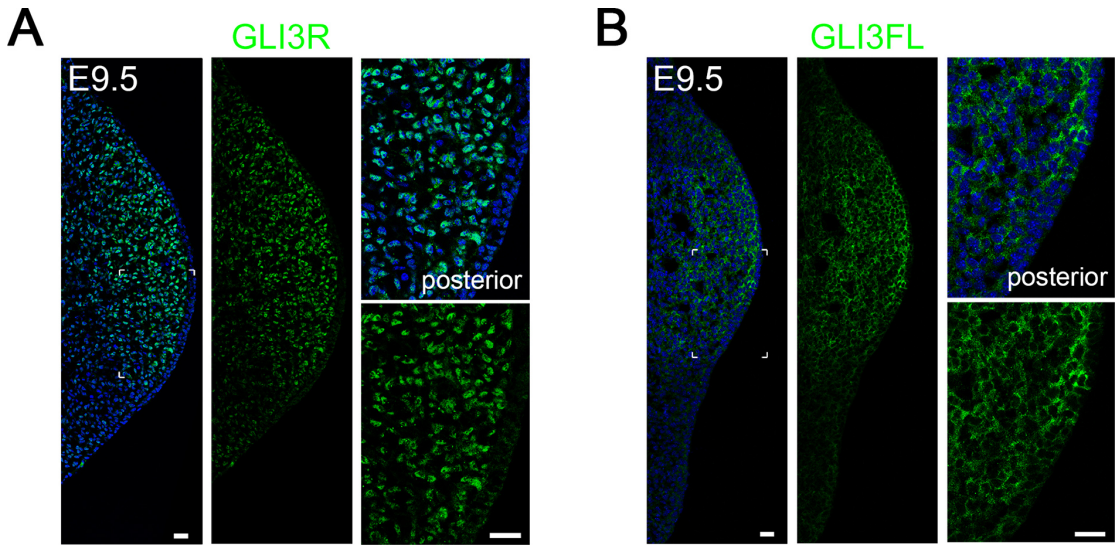

Figure S4 (related to Figure 4). Nuclear GLI3R proteins during the onset of forelimb bud development.

(A) Widespread nuclear GLI3R proteins are detected in the mesenchyme of wild-type forelimb buds during initiation of outgrowth (E9.5, 24-25 somites) using the 6F5 antibody (Wen et al., 2010). (B) In contrast, full-length GLI3^{C3xF} proteins are detected exclusively in the cytoplasm at this stage. This indicates that no detectable nuclear GLI3A proteins are present at this early forelimb bud stage prior to activation of SHH signaling (compare to Figure S1C). Scale bars: 25μm.

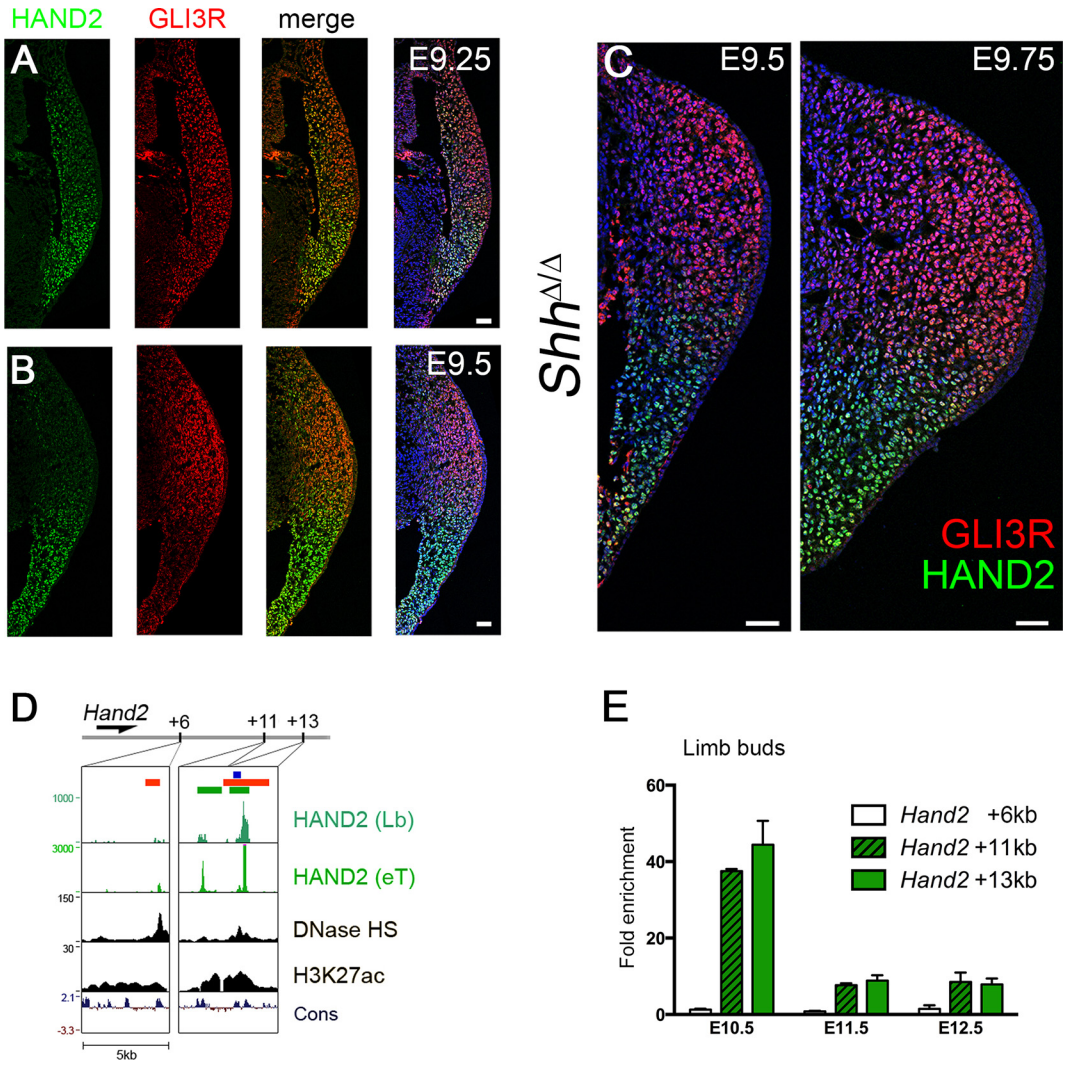

Figure S5 (related to Figure 4). HAND2-mediated AP compartmentalization of the limb bud mesenchyme is *Shh*-independent.

(A, B) HAND2^{3xF} (green) and GLI3R (red) protein distributions in forelimb buds at E9.25 and E9.5 (separate channels of the same limb buds shown in Figure 4A).

(C) HAND2^{3xF} (green) and GLI3R (red) protein distributions in *Shh*-deficient forelimb buds at E9.5 (25-26 somites) and E9.75 (28-29 somites).

(D) ChIP-Seq analysis reveals that HAND2-containing chromatin complexes interact with two genomic regions located 11kb and 13kb downstream of the *Hand2* TSS. A highly conserved element located 6kb downstream served as negative control for the ChIP-qPCR analysis (panel E). Red bars indicate the

regions interacting with GLI3R, whereas the blue bar marks the previously identified CRM with transcriptional repressing activity (Vokes et al., 2008).

(E) Temporal dynamics of the interaction of HAND2-containing chromatin complexes with the *Hand2* +11kb and *Hand2* +13kb candidate CRMs during progression of limb bud development. Fold-enrichments are shown as mean ±SD (n=3).

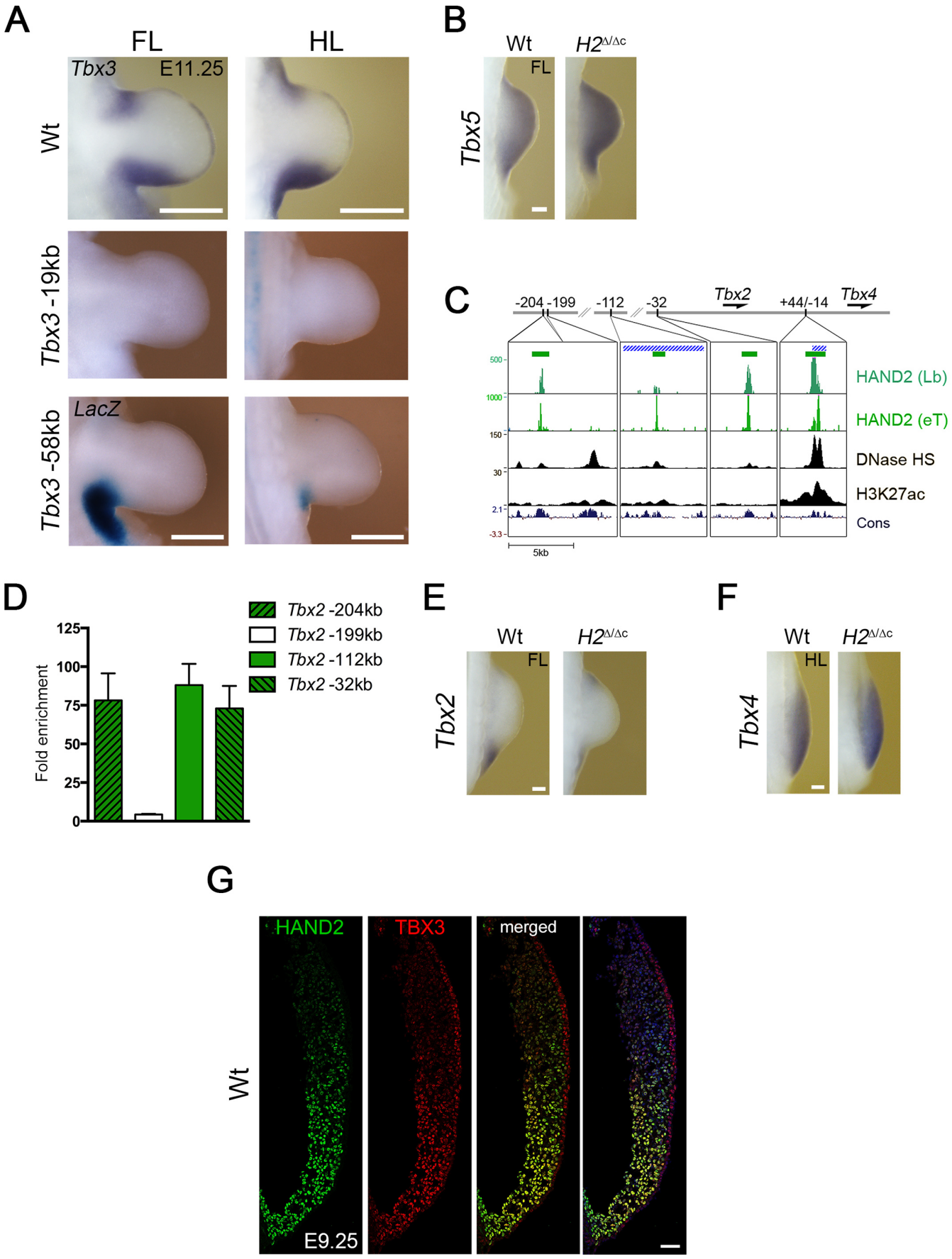
A
FL
HL
Tbx3
E11.25
Wt
Tbx3 -19kb
LacZ
Tbx3 -58kb
B
Wt
H2Δ/Δc
FL
Tbx5
C
-204 -199
-112
-32
Tbx2
+44/-14
Tbx4
500
1000
150
30
2.1
-3.3
HAND2 (Lb)
HAND2 (eT)
DNase HS
H3K27ac
Cons
5kb
D
Fold enrichment
125
100
75
50
25
0
Tbx2 -204kb
Tbx2 -199kb
Tbx2 -112kb
Tbx2 -32kb
E
Wt
H2Δ/Δc
FL
Tbx2
F
Wt
H2Δ/Δc
HL
Tbx4
G
HAND2
TBX3
merged
Wt
E9.25

Figure S6 (related to Figure 5). HAND2-containing chromatin complexes interact with limb bud CRMs in the *Tbx2* -*Tbx4 cis*-regulatory landscape.

(A) *LacZ* reporter activity of the two candidate CRMs located 19kb and 58kb upstream of the *Tbx3* transcription start site in limb buds of transgenic embryos (E11.25) compared to *Tbx3* transcript distribution at the same stage. Scale bar, 500μm. FL: forelimb buds. HL: hindlimb buds.

(B) The forelimb bud-specific expression of *Tbx5* is not altered in *Hand2*$^{\Delta/\Delta c}$ embryos (E10.0, 30-31 somites). Scale bar: 100μm.

(C) HAND2 ChIP-Seq peaks within the *Tbx2*-*Tbx4 cis*-regulatory landscape. HAND2 peaks are detected at 204kb, 112kb and 32kb upstream of the *Tbx2* transcription unit and -14kb upstream of *Tbx4* transcription unit. The striped blue bar overlapping the element located 112kb upstream of *Tbx2* delineates the pDBM59 region that is able to activate *LacZ* expression in the posterior limb bud mesenchyme (Infante et al., 2013). The striped blue bar in the -14kb region upstream of *Tbx4* indicates the hindlimb enhancer that interacts with PITX1 complexes (Infante et al., 2013; Menke et al., 2008).

(D) ChIP-qPCR validates the interaction of HAND2-containing chromatin complexes with the potential CRMs located upstream of the *Tbx2* transcription unit in limb buds at E10.5. The *Tbx2* -199kb region served as a negative control. Mean ±SD is shown (n=3)

(E) *Tbx2* expression in wild-type and *Hand2*$^{\Delta/\Delta c}$ forelimb buds at E9.75 (28-29 somites). Scale bar: 100μm.

(F) The hindlimb bud-specific expression of *Tbx4* is not altered in *Hand2*$^{\Delta/\Delta c}$ embryos (E10.0, 30-31 somites). Scale bar: 100μm.

(G) HAND2^{3xF} (green) and TBX3 (red) protein distributions during initiation of forelimb bud development (E9.25, 22-23 somites). Nuclei appear blue due to counterstaining with Hoechst in the right-most panel. Scale bar: 50μm.

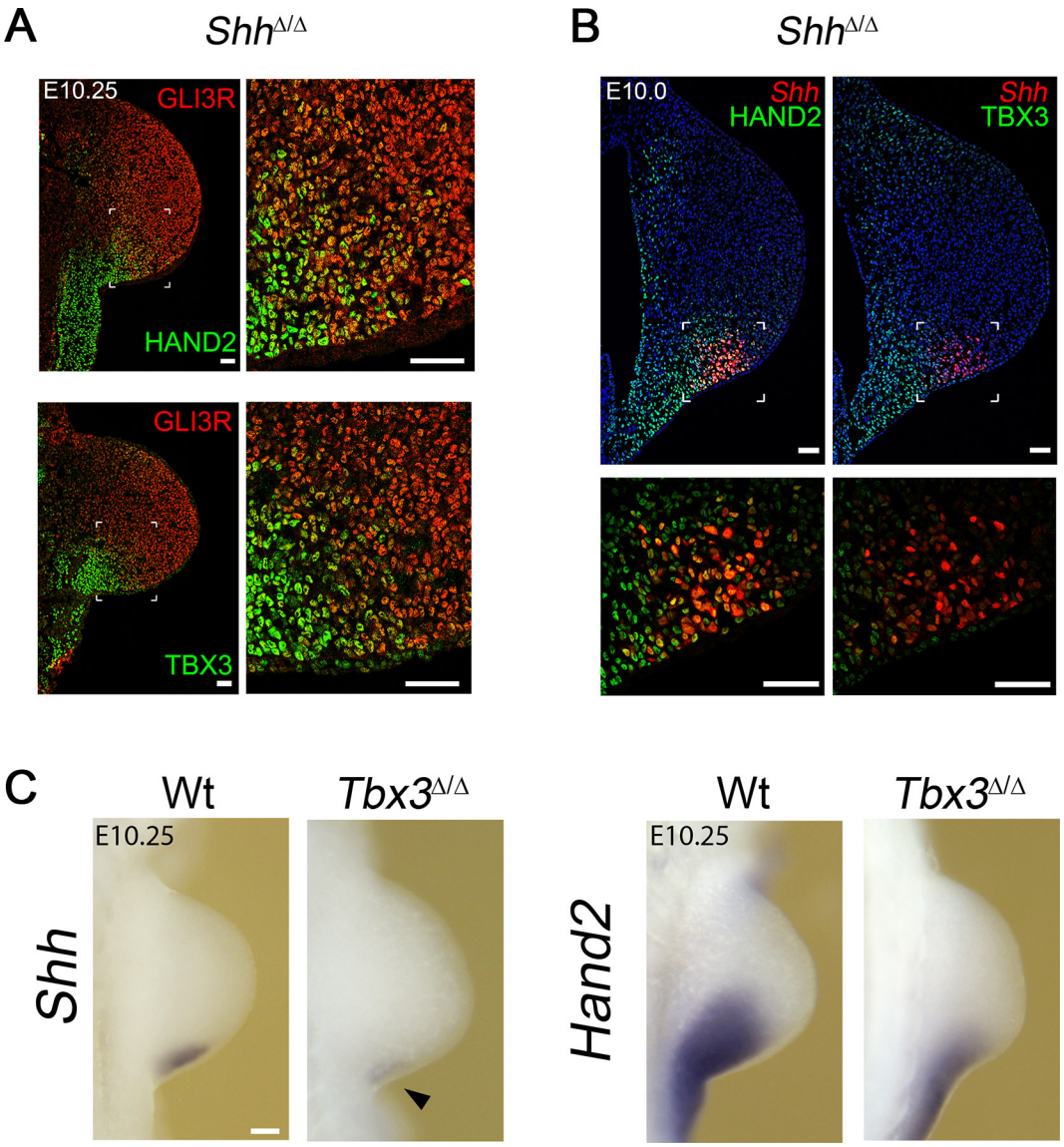

Figure S7 (related to Figure 6). TBX3 participates in restricting GLI3R in *Shh*-deficient limb buds and is dispensable for *Shh* transcription.

(A) Co-localization of GLI3R (red) with HAND2 or TBX3 proteins (green) in *Shh*-deficient forelimb buds (E10.25, 32-33 somites). The enlargements show the GLI3R/HAND2 and GLI3R/TBX3 boundaries in the posterior forelimb bud mesenchyme at single cell resolution. Note that in *Shh*-deficient forelimb buds, the GLI3R protein distribution extends posteriorly to abut the anterior boundary of TBX3 positive cells (see also Figure 6C). In contrast, there is a

significant overlap of the HAND2 and GLI3R protein distributions in the posterior mesenchyme of *Shh*-deficient forelimb buds. Scale bars: 50μm.

(B) Co-localization of cells with active *Shh* transcription (red, revealed using the Shh^{GFPCre} allele) with HAND2 and TBX3 positive nuclei in *Shh*-deficient ($Shh^{GFPCre/GFPCre}$; Harfe et al., 2004) forelimb buds (E10.0, 30-31 somites). This analysis shows that all cells expressing *Shh* are positive for HAND2, but not TBX3 proteins. This result indicates that TBX3 is not *per se* required for activation of *Shh* expression. This is best seen in *Shh*-deficient forelimb buds, as the TBX3 domain is more proximally restricted than in wild-type limb buds. The regions enlarged in the lower panels are indicated in the upper panels. Scale bars: 50μm.

(C) *Shh* and *Hand2* expression in wild-type and *Tbx3*-deficient forelimb buds (n=3/3 at E10.25, 32-33 somites, see also Davenport et al., 2003). A black arrowhead indicates the reduced *Shh* expression domain in *Tbx3*-deficient forelimb buds. This contrasts with the complete loss of *Shh* expression in *Hand2*-deficient limb buds (Galli et al., 2010) and establishes that *Tbx3* is not essential for *Shh* activation in mouse limb buds. The reduction in *Shh* expression in *Tbx3*-deficient forelimb buds is a likely consequence of the more posteriorly restricted *Hand2* expression (right-most panel). Scale bars: 100μm.

Supplemental Tables

Table S1 (related to Figure 2). List of genomic regions enriched ≥2-fold in the HAND2 Lb dataset. Is included as an Excel file.

Table S2 (related to Figure 2). List of genomic regions enriched ≥2-fold in the HAND2 eT dataset. Is included as an Excel file.

Table S3 (related to Figure 2). List of genomic regions enriched ≥8-fold in the HAND2 Lb dataset, sorted according to the weighted number of reads. Top 1000 peaks are shaded grey. Is included as an Excel file.

Table S4 (related to Figure 2). List of genomic regions enriched ≥8-fold in the HAND2 eT dataset, sorted according to the weighted number of reads. Top 1000 peaks are shaded grey. Is included as an Excel file.

Table S5 (related to Figure 2). List of the 259 genomic regions resulting from the intersection of the Lb and eT Top1000 datasets. Is included as an Excel file.

Supplemental Experimental Procedures

Generation of the *Hand2*^{3xFLAG} allele

Mouse embryonic stem cells (ES) carrying a *Hand2* conditional allele (Galli et al., 2010) were used to introduce a 3xFLAG epitope-encoding region into the endogenous locus by using dRMCE. A single 1xFLAG epitope does not provide enough sensitivity to detect endogenous levels of HAND2 protein (Osterwalder et al., 2010). For construction of the exchange vector used in dRMCE, a 3xFLAG coding region was inserted upstream of the *Hand2* start codon. The final exchange cassette was assembled by conventional cloning into a recipient plasmid containing single loxP and FRT sites flanking the engineered *Hand2* locus (exons 1/2 and intervening intron, Figure 1A; Osterwalder et al., 2010). The details of the cloning strategy are available upon request. A step-by-step protocol for dRMCE is available at the Protocol Exchange repository (doi:10.1038/protex.2010.210). Twenty ES clones (16%) were correctly replaced. Germline transmission of the *Hand2*^{3xFLAG} allele was obtained from chimeric mice derived from two independent clones.

Western blot analysis

Fore- and hindlimb buds, heart and branchial arches of single E10.5 embryos (~35-36 somites) were isolated and processed for Western blot analysis (Figure 1B). 15μg of protein extract from each sample was loaded onto 10% SDS-PAGE gels and proteins were subsequently transferred to PVDF membranes (Millipore). HAND2^{3xFLAG} proteins were detected by chemo-luminescence using the monoclonal M2 anti-FLAG antibody (Sigma, F1804) in combination with goat anti-mouse IgG-HRP.

ChIP-qPCR analysis (additional information)

To exclude unspecific effects of the antibody, several genomic regions were assessed in parallel in ChIP-qPCR experiments using wild-type limb buds as starting material, never yielding any significant enrichment (data not shown). An unlinked amplicon targeting the *Actb* locus was used as normalizing control to compute the fold-change enrichment. To prevent artifactual bias of fold enrichments, a cycle threshold of 31 was defined as the minimum background value. Oligos used for qPCR analysis are listed below.

Primers used for ChIP-qPCR analysis

Amplicon	**Forward Primer**	**Reverse Primer**
ZRS 1	5'-TACATTGCCCTCTGGAGTTCA-3'	5'-AGAGGAGAACACAGTGCTGTGA-3'
ZRS 2	5'-AAGCGACATAAACCAGGACAAT-3'	5'-ATAAAGCCAAGCAACATGACAG-3'
ZRS 3	5'-TTCTCTTTAAGATGGAGGCCTG-3'	5'-GGTTTATGTCGCTTTTGGCA-3'
ZRS 4	5'-AATGAACGCTCATGGAGTCC-3'	5'-TGACCAGATGACTTTTCCCC-3'
ZRS 5	5'-GTTCTTTTCCTTGTGATCAG-3'	5'-AAATAGTAAGGACAGGATCG-3'
Gli3 -120kb	5'-ACACACACCAATTTCCCACC-3'	5'-TGGATCCAGCCCAAGTTAGA-3'
Hand2 +6kb	5'-CCTCTGCTTTAATTGCTCCG-3'	5'-CGCTTGTGAATTCACTGCAG-3'
Hand2 +11kb	5'-CCCGCTACTGTATGGCAGAT-3'	5'-TCAGACGACACGACCTGGAT-3'
Hand2 +13kb	5'-GCTTAGTCGCCTTCTCATTG-3'	5'-TAGAGGCTCCCAGTTCTTTG-3'
Id1 +3kb	5'-CACGTTTCCCTCTCTTCCTCT-3'	5'-CTGGGGATGCTCAGGTTAAA-3'
Ets1 -23kb	5'- AGAGTAAACACTTGGGCCGT -3'	5'- GAAGTGTGTGCTGCCTGATT -3'
Ets2 +146kb	5'-TGAGAGAAGTGCATGCCAAC-3'	5'-ATCAGGGAAGCTCAGATCCA-3'
Gsc +33kb	5'-AGCGAAAGTCTAAGCTGCTCTG-3'	5'-AGCGGGAAAGCACCTTTTAA-3'
Gsc -120kb	5'-AGGTTACCCAGCGAACAAAG-3'	5'-GGCATTCTCAGCTGCATTTA-3'
Gsc -133kb	5'-CTGACCTGAGCGTGAGGAA-3'	5'-AGCCTGCTGCTTGTCACC-3'
Tbx18 -338kb	5'-GCGAGTAGGACGCAGATCTTA-3'	5'-CTGTTGGAAGGTGATGACAGA-3'

Tbx18 +174kb	5'-CGGTTGTGAGAGAAGCCAGT-3'	5'-AATGCAACAGGAGGCTGTCT-3'
Irx3 +109kb	5'-CTGCCAAGTTCTTGCAGACA-3'	5'-GGCAATGAGCATTTGACCTT-3'
Irx3 +85kb	5'-CACCTGCTTTTACTTGCTGCT-3'	5'-GGCAGGTTCAAAAGGTGAAA-3'
Tbx3 -59kb	5'-AACTCGGGTACACTCGCACA-3'	5'-ACAGAAAATAAGGCTGGCCC-3'
Tbx3 -58kb	5'-TGTGGTCTGTCACTGTGCACTT-3'	5'-CCAGATTGCCATCACAGACAG-3'
Tbx3 -19kb	5'-TCCCTCAGGAGCTCTGTCTG-3'	5'-AGGATTCCAGGGAGGTCTGT-3'
Tbx2 -204kb	5'-CTCCCACTGATGGCTGAAAT-3'	5'-CCCAGGATGTGAACTGTCAGT-3'
Tbx2 -199kb	5'-CTGTGTGCTACTCCGCATCA-3'	5'-CACTTTCCACTTGGGTGGTG-3'
Tbx2 -112kb	5'-AGGGGAAGGAGGTTAGATGG-3'	5'-GCCTGGGAAGAAAGGCTTC-3'
Tbx2 -32kb	5'-GGCTCGCACCCTCTCTATTA-3'	5'-TTGATCAGCCGTCAGAAACT-3'
Neg	5'-GGATGTGTCACATGCCAATA-3'	5'-AATAGACAATCCCCTAGCCA-3'
Actb +1.8kb	5'-GATCTGAGACATGCAAGGAGTG-3'	5'-GGCCTTGGAGTGTGTATTGAG-3'

ChIP-Seq analysis

For the limb bud (Lb) sample, ~1000 fore- and hindlimb buds from E10.5 *Hand2*^{3xF} embryos were collected in ice-cold PBS. For the *Hand2* expressing tissues (eT) sample, fore- and hindlimb buds with flank mesenchyme, hearts and branchial arches from ~150 *Hand2*^{3xF} embryos or ~150 wild-type controls (E10.5) were pooled. Single nuclei were cross-linked for 5 minutes in 1% formaldehyde. The ChIP-Seq analysis was done using established protocols with minor modifications (Kim et al., 2007; Visel et al., 2009). Sonication was performed on ice using a S-250A Branson sonifier with 3.2mm micro tip (eT sample) or as described for ChIP-qPCR (limb buds; Lb sample). Sonicated chromatin was incubated overnight at 4°C with 10µg of anti-FLAG M2 antibody complexed with protein G-coated Dynabeads (Life Technologies). Immunoprecipitated genomic DNA fragments were purified using the

QIAquick Gel Extraction Kit (Qiagen) and quantified by PicoGreen assays (Life Technologies). In the case of the limb bud (Lb) ChIP-Seq sample, maximally ~2ng of immunoprecipitated chromatin were obtained from ~1000 fine-dissected and pooled fore- and hindlimb buds from *Hand2*^{3xF} homozygote embryos (E10.0-E10.5). In contrast, 7-10ng of immunoprecipitated chromatin was obtained from the expressing tissues of ~150 *Hand2*^{3xF} embryos (E10.5) processed for the eT ChIP-Seq sample. Immunoprecipitated and input (sonicated chromatin) DNA fragments of *Hand2*^{3xF} and wild-type samples were utilized for library construction using the DNA library Prep Kit (New England Biolabs). Following end repair and adaptor ligation, DNA fragments were size selected (200-250bp) by agarose gel electrophoresis and PCR amplified (18 cycles) using Illumina primers. After purification, samples were loaded on an Illumina flow cell for solid-phase amplification. SR50 sequencing of libraries was carried out on a HiSeq 2000 system (Illumina).

ChIP-Seq peak-calling and data analysis

The number of reads sequenced/aligned per sample were as follows:

Sample	Number of reads sequenced	Number of reads mapped to the genome
Lb sample	23,186,136	19,924,323
Lb input sample	117,326,819	95,189,065
eT sample	153,178,049	128,102,911

eT input sample	166,826,821	146,583,591
eT wt sample	139,180,575	87,196,395
eT wt input sample	192,239,694	166,801,906

Reads were mapped to the mouse genome (NCBI37/mm9) using the pipeline described by Stadler et al. (2011) using Bowtie (version 0.12.7; Langmead et al., 2009) with up to 2 mismatches and up to the 100 best alignment positions were reported (bowtie options: -v2 -a --best --strata -m100). For each read a weight of 1.0 was distributed evenly across all the aligned loci with at most two mismatches. In addition, all reads were mapped to RNA annotation databases including RefSeq mRNAs, rRNA, snRNA, snoRNA from GeneBank (2010 release), miRNAs from miRbase (ver. 13), piRNA from NCBI (accessions DQ539889 to DQ569912) and tRNA from http://lowelab.ucsc.edu/GtRNAdb/. Each alignment was weighed by the inverse of the number of hits. In cases where a read had more hits to an individual sequence from one of the annotation databases rather than the whole genome, the former number of hits was selected to ensure that the total weight of a particular read does not exceed 1.0. The sample specific fragment sizes were estimated from the cross-correlation profiles of the read density on both chromosomal strands using the Chipcor software (http://ccg.vital-it.ch/chipseq). Reads were shifted by half of the fragment size (60bp) towards the middle of the fragment. Peaks were detected using MACS (version 1.3.7.1, with parameters --tsize=50 --pvalue=1e-5 --mfold=8 -lambdaset ='1000,5000,10000' --nomodel --shiftsize=60, for details see Zhang et al.,

2008) for the HAND2^{3xF} eT and wild-type control samples in combination with pooled input controls from both samples. A similar pipeline was utilized to detect HAND2^{3xF} binding regions in the Lb ChIP-Seq sample. Peaks were filtered based on the enrichment over the input control samples. ChIP-Seq enrichment of each peak was calculated as e = log2([n_fg /N_fg *min(N_fg,N_bg) + p]/[n_bg /N_bg *min(N_fg,N_bg) + p]), where n_fg and n_bg are the summed weights of overlapping foreground and background (input chromatin) read alignments, respectively. N_fg and N_bg are the total number of aligned reads in foreground and background samples, and p is a pseudo-count constant (p=8) used to minimize the sampling noise for peaks with very low counts.

Only peaks with at least 2-fold enrichment were used for downstream analysis (n=8188 for the Lb dataset, Table S1; n=11072 for the eT dataset, Table S2; identified using a p-value threshold of 1e-5). HAND2^{3xF} peaks were overlapped with the wild-type eT controls and peaks detected in both removed to exclude off-target effects of FLAG antibodies. Peaks called in both the Lb and eT samples are indicated as green bars in schemes. Subsequently, peaks with a $\log_2$ enrichment ≥3 (i.e. over a 8-fold enrichment) with respect to the input (n=5285 for the Lb sample, Table S3; n=4427 for the eT sample, Table S4) were sorted according to the weighted number of reads and the top 1000 Lb and eT peaks with highest enrichments were processed for GREAT analysis (McLean et al., 2010). High-quality reads from E11.5 forelimb H3K27ac (Cotney et al., 2012) and DNaseI HS datasets (UCSC Genome

Browser, Rosenbloom et al., 2013) were mapped to the mouse genome (mm9).

Motif Analysis

To identify the potential binding motif(s) of HAND2 chromatin complexes, we used the Homer software with default settings and various motif widths (ranging from 7 to 10; Heinz et al., 2010)

***In situ* hybridization, skeletal preparations and OPT analysis**

The transcript distribution in mouse embryonic limb buds was assessed by whole mount *in situ* hybridization using digoxigenin-labeled antisense riboprobes (Panman et al., 2006). Minimally, forelimb buds from three independent embryos were analyzed for each stage and genotype (*Hand2*$^{\Delta/\Delta c}$ and *Hand2*$^{\Delta c/+}$ controls) and yielded very similar or identical patterns for all results shown. Cartilage (blue) and bone (red) were visualized by staining embryonic skeletons with Alcian blue and Alizarin red, respectively. For better visualization and orientation of the scapula-humerus articulation, skeletal preparations were embedded in 1% low melting point agarose, dehydrated and cleared in benzyl alcohol-benzyl benzoate for scanning by OPT (Sharpe et al., 2002). An OPT 3001M scanner (Bioptonics, MRC Technology) was used to acquire bright field high-resolution pictures using SkyScan software.

Generation of *LacZ* reporter transgenes and *LacZ* Detection

Candidate enhancer regions were amplified by PCR from mouse genomic DNA and cloned into a *Hsp68*-promoter-*LacZ* reporter vector (Nobrega et al.,

2003). Transgenic mouse embryos were generated by pronuclear injection and founder embryos were stained for *LacZ* activity. It is important to note that the *Hsp68* minimal promoter can result in spurious *LacZ* expression in the ventral neural tube (Gilthorpe and Rigby, 1999). The genomic coordinates of the candidate enhancer regions and the primers used for amplification are listed below.

HAND2^{3xF} peak regions used for *LacZ* transgenic analysis (NCBI37/mm9 mouse genomic assembly)

Genomic region (Vista Browser ID)	**HAND2 ChIP-Seq peak coordinates (eT sample)**	**Coordinates of regions for *LacZ* reporter assays**	**PCR primers used to clone the region for *LacZ* reporter assays**
***Tbx3* -58kb** (mm1177)	chr5:120062062-120062926	chr5:120060938-120063445	F: GGTCCTTGGAGACTGAGACA R: GAATAGCAGAGCACAG Amplicon: 2508bp
***Tbx3* -19kb** (mm1178)	chr5:120101011-120102147	chr5:120100229-120102755	F: GGGGTGAACTGTTGGAGAGA R: TCAGCTAGAGGTCACATGCA Amplicon: 2527bp
***Gli3* -120kb** (mm1179)	chr13:15435051-15435882	chr13:15434540-15436051	F: GAAGAGTGTTACCGGCCTCT R: TCCTCTGTTGTTTTGGCAGC Amplicon: 1512bp
***Irx3 -85*kb** (mm1211)	chr8:94239411-94240209	chr8:94236335-94240424	F: ACCTCAACTTCCATGACACAA

			R: TTGTAACGGTAAATACAGCCCTG Amplicon: 4094 bp

Supplemental References

Amano, T., Sagai, T., Tanabe, H., Mizushina, Y., Nakazawa, H., and Shiroishi, T. (2009). Chromosomal dynamics at the Shh locus: limb bud-specific differential regulation of competence and active transcription. Dev. Cell *16*, 47-57.

Gilthorpe, J.D., and Rigby, P.W.J. (1999). Reporter genes for the study of transcriptional regulation in transgenic mouse embryos. Mol. Embryol. *97*, 159-182.

Heinz, S., Benner, C., Spann, N., Bertolino, E., Lin, Y.C., Laslo, P., Cheng, J.X., Murre, C., Singh, H., and Glass, C.K. (2010). Simple combinations of lineage-determining transcription factors prime cis-regulatory elements required for macrophage and B cell identities. Mol. Cell *38*, 576-589.

Infante, C.R., Park, S., Mihala, A.G., Kingsley, D.M., and Menke, D.B. (2013). Pitx1 broadly associates with limb enhancers and is enriched on hindlimb cis-regulatory elements. Dev. Biol. *374*, 234-244.

Kim, T.H., Barrera, L.O., and Ren, B. (2007). ChIP-chip for genome-wide analysis of protein binding in mammalian cells. Curr. Protocol Mol. Biol. (ed. F.M. Ausubel et al.) *21*, 21.13.

Langmead, B., Trapnell, C., Pop, M., and Salzberg, S.L. (2009). Ultrafast and memory-efficient alignment of short DNA sequences to the human genome. Genome Biol. *10*, R25.

McLean, C.Y., Bristor, D., Hiller, M., Clarke, S.L., Schaar, B.T., Lowe, C.B., Wenger, A.M., and Bejerano, G. (2010). GREAT improves functional interpretation of cis-regulatory regions. Nat. Biotech. *28*, 495-501.

Menke, D.B., Guenther, C., and Kingsley, D.M. (2008). Dual hindlimb control elements in the Tbx4 gene and region-specific control of bone size in vertebrate limbs. Development *135*, 2543-2553.

Nobrega, M.A., Ovcharenko, I., Afzal, V., and Rubin, E.M. (2003). Scanning human gene deserts for long-range enhancers. Science *302*, 413.

Panman, L., Galli, A., Lagarde, N., Michos, O., Soete, G., Zuniga, A., and Zeller, R. (2006). Differential regulation of gene expression in the digit forming area of the mouse limb bud by SHH and gremlin 1/FGF-mediated epithelial-mesenchymal signalling. Development *133*, 3419-3428.

Rosenbloom, K.R., Sloan, C.A., Malladi, V.S., Dreszer, T.R., Learned, K., Kirkup, V.M., Wong, M.C., Maddren, M., Fang, R., Heitner, S.G.*, et al.* (2013). ENCODE data in the UCSC Genome Browser: year 5 update. Nucl. Acids Res. *41*, D56-63.

Sharpe, J., Ahlgren, U., Perry, P., Hill, B., Ross, A., Hecksher-Sorensen, J., Baldock, R., and Davidson, D. (2002). Optical projection tomography as a tool for 3D microscopy and gene expression studies. Science *296*, 541-545.

Stadler, M.B., Murr, R., Burger, L., Ivanek, R., Lienert, F., Scholer, A., van Nimwegen, E., Wirbelauer, C., Oakeley, E.J., Gaidatzis, D.*, et al.* (2011). DNA-binding factors shape the mouse methylome at distal regulatory regions. Nature *480*, 490-495.

Visel, A., Blow, M.J., Li, Z., Zhang, T., Akiyama, J.A., Holt, A., Plajzer-Frick, I., Shoukry, M., Wright, C., Chen, F.*, et al.* (2009). ChIP-seq accurately predicts tissue-specific activity of enhancers. Nature *457*, 854-858.

Zhang, Y., Liu, T., Meyer, C.A., Eeckhoute, J., Johnson, D.S., Bernstein, B.E., Nusbaum, C., Myers, R.M., Brown, M., Li, W.*, et al.* (2008). Model-based analysis of ChIP-Seq (MACS). Genome Biol *9*, R137.